Comparison of Distributed Parameter and Multi-lump Models for a Pressurized Water Reactor Core

by

Taipeng Zhang

A Thesis Presented in Partial Fulfillment
of the Requirements for the Degree
Master of Science

Approved November 2012 by the
Graduate Supervisory Committee:

Keith E. Holbert, Chair
Vijay Vittal
Daniel Tylavsky

ARIZONA STATE UNIVERSITY

December 2012

ABSTRACT

A distributed-parameter model is developed for a pressurized water reactor (PWR) in order to analyze the frequency behavior of the nuclear reactor. The model is built based upon the partial differential equations describing heat transfer and fluid flow in the reactor core. As a comparison, a multi-lump reactor core model with five fuel lumps and ten coolant lumps using Mann's model is employed. The derivations of the different transfer functions in both models are also presented with emphasis on the distributed parameter. In order to contrast the two models, Bode plots of the transfer functions are generated using data from the Palo Verde Nuclear Generating Station. Further, a detailed contradistinction between these two models is presented.

From the comparison, the features of both models are presented. The distributed parameter model has the ability to offer an accurate transfer function at any location throughout the reactor core. In contrast, the multi-lump parameter model can only provide the average value in a given region (lump). Also, in the distributed parameter model only the feedback according to the specific location under study is incorporated into the transfer function; whereas the transfer functions derived from the multi-lump model contain the average feedback effects happening all over the reactor core.

For my parents

Tongqi Zhang & Shuang Su

ACKNOWLEDGEMENTS

I wish to take this opportunity to show my appreciation to my committee chair, Professor Keith E. Holbert for his invaluable support and guidance on this thesis. His expertise in this area supplied a solid foundation for this research and his patient instruction led to the successful result. I wish to thank Professor Vijay Vittal and Professor Daniel Tylavsky for their help and being the committee members. I would also like to thank my parents, friends, advisors, secretaries and other administrative personnel associated with School of Electrical, Computer and Energy Engineering and the Graduate College for their great support.

TABLE OF CONTENTS

Page

LIST OF TABLES vii

LIST OF FIGURES viii

NOMENCLATURE..... xi

CHAPTER

I INTRODUCTION 1

II BACKGROUND OVERVIEW 3

Fundamentals of Nuclear Reactor 3

Prompt Neutrons 3

Delayed Neutrons 5

Reactivity 6

Reactor Period 7

Point Kinetics 7

Zero Power Reactor Transfer Function 9

Reactivity Feedback Mechanisms 10

Fuel Temperature Coefficient of Reactivity 11

Moderator Temperature Coefficient of Reactivity 13

Reactor Core Modeling 13

III MULTI-LUMP MODEL 15

Theory 15

CHAPTER Page

Mann's Model 16

Frequency Response 20

Modeling and Simulation 21

Reactivity Change as Input 23

Coolant Inlet Temperature Change as Input 31

Fuel Temperature to Power Transfer Function in Both Cases 36

IV THEORY 39

General Distributed Method 39

Distributed-Parameter Model of PWR 40

Fuel Rod Temperature 41

Coolant Temperature and Flow 44

Combined Fuel and Coolant 47

V MODELING AND SIMULATION 49

Modeling 49

Simulation 51

Individual Transfer Functions 51

Pure Time Delay 60

Combined Transfer Functions 61

IV CONCLUSIONS AND RECOMMENDATIONS 74

Page

REFERENCES 77

APPENDIX

A PARAMETERS FOR PALO VERDE NUCLEAR GENERATING STATION 79

LIST OF TABLES

TABLE Page

2.1 Relationship among *k*, ρ and criticality.....6

3.1 Time constants and their corresponding frequencies….....……...27

A Parameters for Palo Verde Nuclear Generating Station.....80

LIST OF FIGURES

Figure Page

2.1. Doppler broadening……...……12

3.1. Block diagram of the multi-axial lump reactor core model……...15

3.2. Block diagram of Mann's model……16

3.3. Block diagram of Mann's model with multiple lumps……..20

3.4. Multi fuel-coolant node model……...22

3.5. Power to reactivity transfer function……..24

3.6. Fuel temperature at the upmost lump to reactivity transfer function…….27

3.7. Fuel temperature at the upmost lump to reactivity transfer function with data cursor……..28

3.8. Comparison of different α values……..29

3.9. Coolant exit temperature to reactivity transfer function……30

3.10. Coolant exit temperature to power transfer function…….....31

3.11. Coolant exit temperature to fuel temperature at the upmost lump transfer function…….....….....32

3.12. Power to coolant inlet temperature transfer function…….33

3.13. Fuel temperature at the upmost lump to coolant inlet temperature transfer function……..34

3.14. Coolant exit to inlet temperature transfer function-reactivity……35

3.15. Coolant lump temperature to coolant inlet temperature……36

Figure Page

3.16. Fuel temperature at the upmost lump to power transfer function-reactivity……37

3.17. Fuel temperature at the upmost lump to power transfer function-coolant inlet temperature……..38

4.1. Distributed-parameter model of a PWR……41

4.2. Transfer functions between variables where the number in brackets refers to the equation number derived in the text……..48

5.1. The overall block diagram of the PWR distributed parameter model…...50

5.2. Zero-power reactor transfer function……52

5.3. Fuel temperature to power transfer function - distributed-parameter……53

5.4. Fuel temperature to power transfer function – multi node……54

5.5. Coolant temperature to fuel heat production transfer function…….55

5.6. Part of coolant temperature to fuel temperature transfer function…….56

5.7. Part of the coolant temperature to power transfer function……...57

5.8. Coolant temperature at height *z* to coolant inlet temperature - distributed-parameter log-log scale…….58

5.9. Coolant lump temperature to coolant inlet temperature – multi node…..59

5.10. Coolant temperature at height *z* to coolant inlet temperature - distributed-parameter compare……5

Figure Page

5.11. Pure time delay of $\tau_R = 0.76219$ sec……..61

5.12. Overall power to reactivity transfer function - distributed-parameter…...63

5.13. Overall power to reactivity transfer function - multi node……63

5.14. Power to coolant inlet temperature transfer function - distributed-parameter……...64

5.15. Power to coolant inlet temperature transfer function - multi node……65

5.16. Coolant temperature at height *z* to power transfer function - distributed-parameter……...66

5.17. Coolant exit temperature to power transfer function - multi node…….67

5.18. Coolant temperature to fuel temperature transfer function - distributed-parameter……...68

5.19. Coolant exit temperature to fuel temperature at the upmost lump transfer function - multi node……69

5.20. Fuel temperature to reactivity transfer function - distributed-parameter...70

5.21. Fuel temperature at the upmost lump to reactivity transfer function - multi node……..71

5.22. Coolant temperature to reactivity transfer function - distributed-parameter……...72

5.23. Coolant exit temperature to reactivity transfer function - multi node…..73

NOMENCLATURE

A	cross-sectional flow area of the coolant channel
A_{FC}	effective heat transfer surface area of the fuel rod
B^2	buckling
c_C , c_{pc}	specific heat of the coolant
c_F , c_{pF}	specific heat of the fuel
C	delayed neutron precursor concentration
$C(\vec{r},t)$	a forcing function (non-homogeneous term)
D	diffusion coefficient
E_{C1}	heat energy in the first (inlet) coolant lump
E_F	heat energy in the fuel lump
E_R	recoverable energy
f	thermal utilization
h	fuel rod surface heat transfer coefficient
I	resonance integral
k	multiplication factor
l	neutron lifetime
l_{Avg}	average thermal neutron lifetime accounts for delayed neutrons
l_p	prompt lifetime
L_r	linear differential operator containing all derivatives with respect to

position and all constants

$\mathcal{L}_{\text{th}}$ thermal nonleakage probability

m_C mass of the coolant in the core

$\dot{m}_C$ coolant mass flow rate in the core

m_F mass of the fuel in the core

$(\text{mfp})_a$ mean free path to absorption

M_t a linear differential operator containing all derivatives with respect to time

n_0 initial number of neutrons

$n_i(t)$ number of neutrons in the *i*th generation

P heated perimeter of the coolant channel

P_0 the steady-state power generated in core

$\wp$ resonance escape probability

Q_C volumetric heat generation in coolant

Q_F heat generation rate per unit volume in the fuel rod

$\vec{r}$ position vector

r_0 radius of the cylindrical fuel rod

t_d mean neutron diffusion time

t_d^M mean neutron diffusion time of the moderator

$t_{1/2}$ radioactive half-life

T	reactor period
T_F	fuel temperature
T_M	moderator temperature
T_0	temperature in the material at $r = r_0$
u	coolant velocity
U_{FC}	overall fuel-to-coolant heat transfer coefficient
V	volume of the reactor core
z	axial position
α_M	moderator temperature reactivity feedback coefficient
α_T	temperature reactivity feedback coefficient
α_T^F, α_F	fuel temperature reactivity feedback coefficient
β	delayed neutron fraction
θ_i	average temperature of the *i*th coolant lump
θ_{in}	coolant inlet temperature
θ_{out}	coolant outlet temperature
Θ	temperature of the coolant
λ	delayed neutron precursor decay constant
Λ	neutron generation time
ρ	reactivity
ρ_c	coolant density

ρ_{ext} external reactivity input

ρ_F fuel density

Σ_a macroscopic absorption cross-section

$\overline{\Sigma}_a$ thermal macroscopic absorption cross-section

$\overline{\Sigma}_a^F$ thermal macroscopic absorption cross-section of the fuel

$\overline{\Sigma}_a^M$ thermal macroscopic absorption cross-section of the moderator

τ average (or mean) life of a radionuclide

τ_C coolant to fuel heat transfer time constant

τ_F fuel to coolant heat transfer time constant

τ_R coolant residence time in the core

ϕ neutron flux

CHAPTER I

INTRODUCTION

This thesis describes a distributed-parameter model using partial differential equations for the pressurized water reactor (PWR). This model is used to analyze the frequency behavior of the nuclear power reactor.

Previous researchers have developed methods based on different multi-lump parameter models to evaluate the behavior of the nuclear reactor core. A result has been reached that the more lumps the model has, the more accurate the results are. However, the multi-lump model is based on the average theory; it is difficult to arrive at a very accurate result at any exact point that is going to be studied. To increase the model resolution, the number of lumps could be increased to a very large number. But this makes an analytical calculation very complicated and may take a large amount of (computer) time to solve the huge matrix.

This is an impetus to build a distributed-parameter model so that wherever the location of interest, the actual value at that exact position can be calculated. With the distributed-parameter model, the transfer function between any input and output at any location throughout the reactor core can be derived, plotted and analyzed. This makes the result more accurate yet the calculation is more simplified. This research simulates the transfer functions by producing the Bode plots using MATLAB. This research shows that the distributed parameter model is

correct and more accurate than the multi-lump model. By plotting the same transfer function at different locations in the same graph, it helps to have a better understanding of the response and behavior of the reactor core.

Chapter II provides background information on nuclear power plants and the nuclear reactor core. The zero power transfer function and the feedback mechanisms are also reviewed. The different nuclear reactor modeling methods are briefly introduced and compared at the end of Chapter II. Chapter III explains the theory of multi-lump reactor core modeling. A multi-lump model with five fuel lumps and ten coolant lumps is established using Mann's model. Analysis is made by graphing the Bode plot of the transfer functions with MATLAB using data from the Palo Verde Nuclear Generating Station [1] [2]. In Chapter IV the general distributed parameter modeling theory is introduced. Then, a distributed-parameter model of a PWR is built and its transfer functions are derived. Chapter V simulates the distributed-parameter model established in Chapter IV with MATLAB using the same nuclear power plant data used in Chapter III. The comparison of two models is made and the differences between them are analyzed and explained. Chapter VI summarizes the research accomplishments and presents recommendations for future work.

CHAPTER II

BACKGROUND OVERVIEW

This research mainly deals with the modeling and transfer functions of the nuclear reactor core. To have a better understanding, some basic nuclear reactor knowledge will be explained in this chapter. Feedback mechanisms are very important in a nuclear reactor, so the different feedback paths and coefficients are also covered. Since most of the analysis is based on modeling, some existing modeling methods will be discussed.

Fundamentals of Nuclear Reactor

Prompt Neutrons

The reactor kinetics describe the time dependent neutronic behavior of the reactor by itself. The neutron population changes from one generation to the next based on the multiplication factor *k*. The number of neutrons in the *i*th generation $n_i(t)$ can be expressed as: $n_i(t) = n_0 k^i$, where n_0 is the initial number of neutrons. The period between one neutron generation to the next is defined as the neutron lifetime (*l*). There are two major stages that a thermal neutron goes through from its birth to death: slowing down from fast to thermal energy; and diffusion until being absorbed or leaking out. The latter one dominates the time period and it depends on the specific moderator material. The lifetime of a prompt

neutron in an infinite reactor is: $l_p^{\infty} = \frac{\text{distance}}{\text{velocity}} = \frac{(\text{mfp})_a}{v} = \frac{1}{v\Sigma_a}$, where $(\text{mfp})_a$ is the mean free path to absorption and Σ_a is the macroscopic absorption cross-section [3]. By employing the Maxwellian neutron distribution, the prompt neutron lifetime in a thermal reactor can be estimated as the mean neutron diffusion time (t_d): $l_p^{\infty} \cong t_d = \frac{1}{\Sigma_a(E_0)v_0} = \frac{\sqrt{\pi}}{2v_T\overline{\Sigma}_a}$, where $\overline{\Sigma}_a$ is the thermal macroscopic absorption cross-section. In the case of a moderator-fuel mixture, the mean neutron diffusion time can be calculated as: $t_d = \frac{\sqrt{\pi}}{2v_T\left(\overline{\Sigma}_a^F + \overline{\Sigma}_a^M\right)} = \frac{\sqrt{\pi}}{2v_T\overline{\Sigma}_a^M}\left(\frac{\overline{\Sigma}_a^M}{\overline{\Sigma}_a^F + \overline{\Sigma}_a^M}\right) = t_d^M(1-f)$, where $\overline{\Sigma}_a^F$ is the thermal macroscopic absorption cross-section of the fuel, $\overline{\Sigma}_a^M$ is the thermal macroscopic absorption cross-section of the moderator, t_d^M is the mean neutron diffusion time of the moderator and *f* is the thermal utilization [4].

Note that in actuality, the reactor cannot be an infinite core. Thus, absorption is not the only way of a neutron's death; they may leak out from the core as well. In the finite reactor, only the neutrons that remain in the core contribute to the prompt lifetime (l_p): $l_p = l_p^{\infty}\mathcal{L}_{\text{th}}$, where $\mathcal{L}_{\text{th}}$ is the thermal nonleakage probability.

The neutron generation time (Λ) is defined as the time period from birth (fission) to absorption-inducing fission (death) as a replacement to the neutron lifetime: $\Lambda = \frac{l}{k}$, where *k* is the multiplication factor describing criticality. From

the equation above, it can be seen that when $k = 1$, that is when the reactor is critical, the lifetime and the generation time are equal.

Delayed Neutrons

Besides prompt neutrons, the other important group of neutrons is the delayed neutrons. Radioisotopes decay by different mechanisms. Most of them are by alpha and beta decay. However, some neutron-rich radionuclides decay by neutron emission: ${}^{A}_{Z}P \rightarrow {}^{A-1}_{Z}D + {}^{1}_{0}n$, where *P* means the parent, *D* means the daughter and the *n* is the neutron. Delayed neutrons come from decay chains which have one or more beta emitters prior to the neutron emitter. Almost the entire delay time until the delayed neutron appears comes from the beta decay while only a little amount, which could be neglected, is from the actual delayed neutron emission. Then, the delayed neutron precursor (*C*) is defined as the radioactive fission product progeny that decays by neutron emission.

The delayed neutrons are emitted from some fission products, but the delayed neutron fraction (β) is very small, typically less than 1% [5]. However, the importance of the delayed neutron cannot be overemphasized since without them, the nuclear reactor would be uncontrollable. Therefore, the delayed neutrons are sure very important for a thermal reactor.

Each radionuclide has its own decay constant (λ): $\lambda = \frac{\ln(2)}{t_{1/2}}$, where $t_{1/2}$ is

the half-life [6]. The average (or mean) life of a radionuclide (τ) is defined as: $\tau = \frac{1}{\lambda}$. Then, the average thermal neutron lifetime accounts for delayed neutrons can be calculated as:

$$l_{Avg} = (1-\beta)l_p + \beta(\frac{1}{\lambda} + l_p) \cong \frac{\beta}{\lambda} = \beta\tau \quad (2.1)$$

Reactivity

Reactivity (ρ) is used to describe the change is criticality. It is defined as: $\rho = \frac{k-1}{k} = \frac{\Delta k}{k}$ [7]. The relationship among *k*, ρ and criticality is shown as Table 2.1. Reactivity can be expressed as a dimensionless quantity or in units of dollars: $\$ \equiv \frac{\rho}{\beta}$. Note that a dollar of reactivity is very large. Usually, a smaller unit, the cent, is used to quantify the amount of reactivity [8].

Table 2.1 Relationship among *k*, ρ and criticality

Multiplication Factor	Reactivity	Condition
$k < 1$	$\rho < 0$	Subcritical
$k = 1$	$\rho = 0$	Critical
$k > 1$	$\rho > 0$	Super Critical
$k(1-\beta) > 1$	$\rho > \beta$	(Super) prompt critical

Reactor Period

The reactor period (T) is defined as: $\frac{1}{T} = \frac{1}{n}\frac{dn}{dt}$. The time required for the flux or power to increase by a factor of e (e = 2.728) is also called the stable reactor period. For very small reactivity changes ($\rho << \beta$), $T \cong \frac{l_{Avg}}{\rho} \cong \frac{\beta}{\lambda\rho} = \frac{\beta\tau}{\rho}$. For large positive reactivity insertions ($\rho >> \beta$), $T \cong \frac{l_p}{\rho - \beta}$, which is a (super) prompt critical condition [9].

Point Kinetics

Now, the set of differential equations that describe the time-dependent neutron population including the delayed neutrons is derived. The derivation begins with the expression: $\frac{\partial n}{\partial t} = \text{Production} - \text{Leakage} - \text{Absorption}$. So, the basic neutron balance becomes

$$\frac{\partial n}{\partial t} = \left[\left(1-\beta\right)\nu\Sigma_f\phi + \lambda C\right] - DB^2\phi - \Sigma_a\phi \qquad (2.2)$$

where B^2 is buckling and D is the diffusion coefficient. Since the flux $\phi = n\mathrm{v}$, take the derivative of the equation and get:

$$\frac{d\phi}{dt} = \mathrm{v}\frac{dn}{dt} \qquad (2.3)$$

Substitute Equation (2.3) into Equation (2.2) and rearrange, it yields to:

$$\frac{d\phi}{dt} = \mathrm{v}\nu\Sigma_f \left[(1-\beta) - \frac{DB^2 + \Sigma_a}{\nu\Sigma_f} \right] \phi + \mathrm{v}\lambda C \tag{2.4}$$

Equation (2.4) can be simplified as:

$$\frac{d\phi}{dt} = \mathrm{v}\nu\Sigma_f (\rho - \beta)\phi + \lambda(\mathrm{v}C) \tag{2.5}$$

Define $C' = \mathrm{v}C$, so Equation (2.5) can be re-written as:

$$\frac{d\phi}{dt} = \frac{1}{\Lambda}(\rho - \beta)\phi + \lambda C' \tag{2.6}$$

For the delayed neutron precursors, the differential equation is:

$$\frac{dC}{dt} = \nu\beta\Sigma_f\phi - \lambda C \tag{2.7}$$

Multiply Equation (2.7) by a factor of v and have:

$$\mathrm{v}\frac{dC}{dt} = \mathrm{v}\nu\beta\Sigma_f\phi - \lambda \mathrm{v}C \tag{2.8}$$

Substitute $C' = \mathrm{v}C$ into Equation (2.8) and simplify it to:

$$\frac{dC'}{dt} = \frac{1}{\Lambda}\beta\phi - \lambda C' \tag{2.9}$$

Equations (2.6) and (2.9) are the final version of the *generation time formulation* of the point kinetics equations that includes the delayed neutron contribution.

Since $P = E_R\Sigma_f V\phi$, the *point kinetics equations* can be re-written in the power form as:

$$\frac{dP}{dt} = \frac{1}{\Lambda}(\rho - \beta)P + \lambda C'' \tag{2.10}$$

$$\frac{dC''}{dt} = \frac{1}{\Lambda}\beta P - \lambda C'' \tag{2.11}$$

where $C'' = E_R \Sigma_f VC$, and E_R and V are the recoverable energy and volume of the reactor core, respectively [10].

Zero Power Reactor Transfer Function

Transfer functions are very important in examining system response based on the changes in a single input parameter. The response is the output and in a nuclear reactor, it is usually power (P) or flux (ϕ) while the input variable is the reactivity (ρ). So, the transfer function (G) can be written as:

$$G(s) = \frac{Output}{Input} = \frac{P(s)}{\rho(s)} \tag{2.12}$$

Equation (2.12) is referred to as the zero power reactor transfer function because an assumption has been made that no feedback mechanisms are present. In order to make this assumption reasonable, the reactor should be at such a low power that the temperatures of the fuel and moderator do not increase above the ambient temperature.

Since the product of power and reactivity is nonlinear, the point kinetics equation cannot be used directly. Thus, the perturbation form of the point kinetics equations shall be used. The linearized point kinetic equations can be used to determine the transfer function of the zero power reactor. Equation (2.13) shows

the zero power reactor transfer function with a single delayed neutron precursor group in terms of power [11].

$$G_0(s) = \frac{\delta P(s) / P_0}{\delta \rho(s)} = \frac{s + \lambda}{s\Lambda\left(s + \lambda + \frac{\beta}{\Lambda} \right)} \tag{2.13}$$

Substitute $s = j\omega$ into Equation (2.13), the zero power reactor transfer function in terms of frequency (ω in radians/second) can be written as:

$$G_0(\omega) = \frac{\delta P(\omega) / P_0}{\delta \rho(\omega)} = \frac{j\omega + \lambda}{j\omega\Lambda\left(j\omega + \lambda + \frac{\beta}{\Lambda} \right)} \tag{2.14}$$

Equation (2.14) shows that the zero power reactor transfer function has one zero at $\omega = \lambda$ and two poles at $\omega = 0$ and $\omega = \lambda + \frac{\beta}{\Lambda}$.

Reactivity Feedback Mechanisms

The zero power reactor transfer function describes the response based only on the point kinetics equations. However, in a real nuclear power reactor, feedback influences must be considered in order to fully characterize the reactor behavior. The feedback is from both internal and external mechanisms. The internal factors include fuel heat element heat transfer, changes in coolant density, pressure, phase boundaries, acceleration, and effects of temperature and coolant density on reactor reactivity. The external effects are load conditions and other equipment like pressurizer, steam generator, etc.

There are four inherent reactivity feedback mechanisms of significant magnitude, including: [12]

1. Fuel temperature (Doppler) coefficient;
2. Moderator temperature coefficient;
3. Moderator void coefficient; and
4. Moderator pressure coefficient.

Only the first two reactivity feedback coefficients of temperature are utilized in this work. The temperature reactivity feedback coefficient (α_T) is defined as below:

$$\alpha_T \equiv \frac{d\rho}{dT} = \frac{1}{k^2}\frac{dk}{dT} \cong \frac{1}{k}\frac{dk}{dT} \tag{2.15}$$

In order to have a stable reactor operation, the reactivity feedback coefficients must be negative. And the reactivity coefficients are not constants, they change over the core life.

Fuel Temperature Coefficient of Reactivity

The mechanism behind the fuel temperature coefficient of reactivity is Doppler broadening, which means an increase in fuel temperature (*T*) causes a broadening of the resonance cross sections with a corresponding decrease in the self-shielding and an increase in the resonance absorption, shown as Figure 2.1. Note that even though the peak in the figure decreases with the increase of the

temperature, the area under the absorption cross section curve remains the same. The Doppler effect is very important because it is fast acting and it is usually negative.

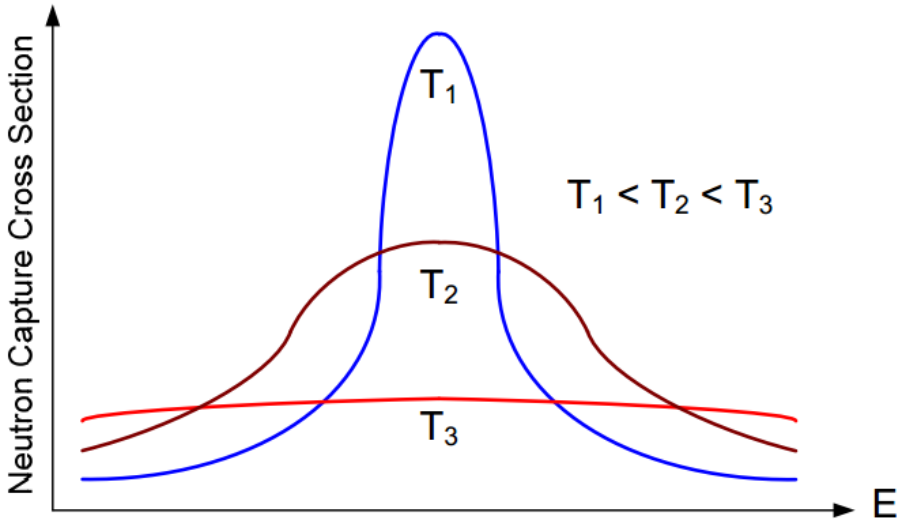

Fig. 2.1 Doppler broadening.

According the definition of the temperature reactivity feedback coefficient (Equation 2.15), the fuel temperature reactivity feedback coefficient α_T^F is defined as:

$$\alpha_T^F = \frac{1}{k}\frac{dk}{dT_F} = \ln(\wp)\frac{1}{I}\frac{dI}{dT_F} \tag{2.16}$$

where $\wp$ is the resonance escape probability and I is the resonance integral. Considering the resonance integral temperature dependence leads to:

$$\frac{dI(T_F)}{dT_F} = \frac{d}{dT_F} I(300K)\left[1+\beta_I\left(\sqrt{T_F}-\sqrt{300K}\right)\right] = \frac{I(300K)\beta_I}{2\sqrt{T_F}} \tag{2.17}$$

where $\beta_I = A' + \frac{C'}{r_F \rho_F}$ and A', C' are constants. Substitute Equation (2.17)

into Equation (2.16) and we obtain: [13]

$$\alpha_T^F = \frac{-\beta_I}{2\sqrt{T_F}} \ln\left[\frac{1}{\wp(300K)}\right] \tag{2.18}$$

Moderator Temperature Coefficient of Reactivity

The moderator temperature coefficient (MTC) of reactivity, typically designated as α_M, is defined as the change in reactivity ρ per unit change in the moderator temperature T_M:

$$\alpha_M = \frac{d\rho}{dT_M} \tag{2.19}$$

It is a very important reactivity coefficient in the nuclear reactor core. In a typical PWR, water is used as both coolant and moderator. So, in this thesis, coolant and moderator are the same.

Reactor Core Modeling

Now, the linearized point kinetics equations for a pressurized water reactor can be re-written considering the fuel temperature coefficient and the moderator temperature coefficient:

$$\frac{d\delta P}{dt} = \frac{-\beta_T}{\Lambda}\delta P + \lambda\delta C + \frac{\alpha_F P_0}{\Lambda}\delta T_F + \frac{\alpha_M P_0}{\Lambda}\delta T_M + \frac{P_0}{\Lambda}\delta\rho_{ext} \tag{2.20}$$

$$\frac{d\delta C}{dt} = \frac{\beta_T}{\Lambda}\delta P - \lambda\delta C \tag{2.21}$$

where P_0 is the reactor power and ρ_{ext} is an external reactivity input (e.g., control rod).

Researchers have divided the nuclear reactor core into a fuel lump and a coolant (moderator) lump in order to study the response of the reactor. However, they found that this model cannot provide an accurate result because the parameters are changing throughout the core. So, the multi-lump model was created. Multi-lump means that the fuel and coolant has been divided into different lumps, typically according to the height. At first, there is only one coolant lump for each fuel lump. It is still not accurate enough. Therefore, a multi-lump model which uses two coolant lumps for each fuel lump has been made, known as the Mann's model [14]. Mann's model has increased the accuracy of the study and it can get a better result just by increasing the number of lumps. However, it is still based on an average method and if the number of lumps gets too big, this makes it hard to solve the huge matrix which may take a large amount of (computer) time during calculation. So it is useful to create a distributed parameter model so that wherever the point is of interest, the actual value at that exact position can be calculated. And with the distributed parameter model, the transfer functions between any two parameters at any place in the core can be derived, calculated and plotted very accurately. This thesis will present both models and make a detailed comparison between them.

CHAPTER III

MULTI-LUMP MODEL

In order to generate a more detailed reactor core model compared to the single lump reactor core model, the multi-lump reactor core model has been established. In this model, more than one lump is used to describe the fuel and coolant interactions in the core.

Theory

In the multi-lump reactor core model, the lump may be divided in either the radial or axial direction as well as the fuel to coolant heat transfer. Obvious divisions are the cladding, gap and the fuel pellet itself. However, because of the relative size difference between these three components, it is the fuel rod that is generally divided into several sections. Figure 3.1 shows the block diagram of a typical multi-lump reactor core with *N* fuel lumps and *N* coolant lumps.

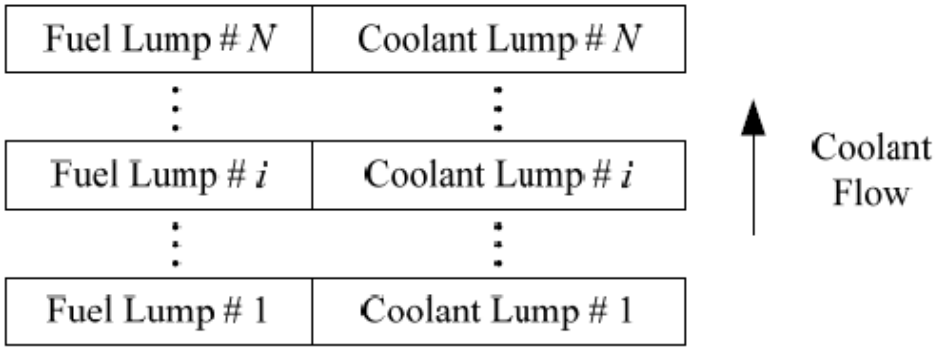

Fig. 3.1 Block diagram of the multi-axial lump reactor core model.

Mann's Model

One of the problems brought by the modeling of the heat transfer process is the value of the driving temperature difference (ΔT). Mann's model uses two coolant lumps for each fuel lump. Thus, ΔT is then changed into the temperature difference between the fuel and the average temperature of the first coolant lump. Here, an assumption is made that each coolant lump is well-stirred so that the outlet coolant temperature equals the average coolant temperature in the lump. Figure 3.2 shows the block diagram of Mann's Model [14].

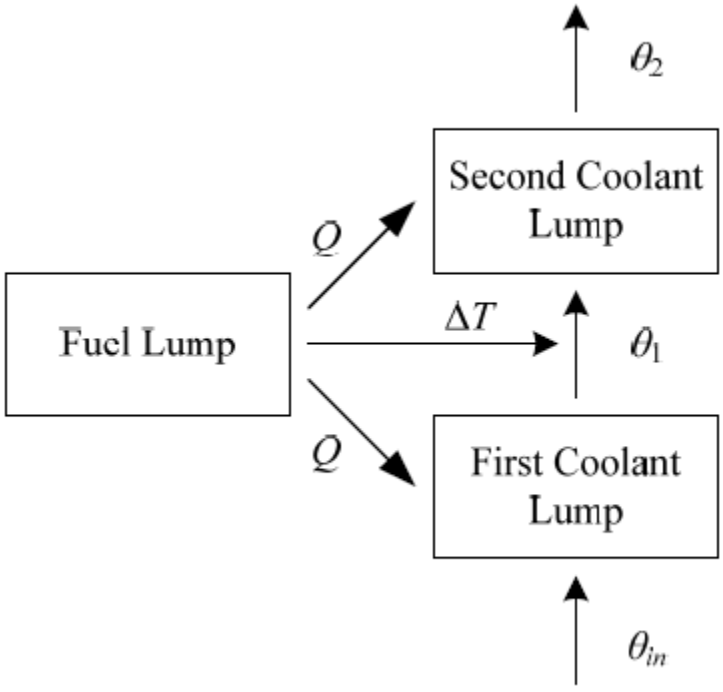

Fig. 3.2 Block diagram of Mann's model.

The advantage of Mann's model is that it provides a more realistic representation for the heat transfer from the fuel to the coolant, compared with

using the single coolant lump which assumes that the average coolant temperature (T_{avg}) in the lump is the mean value of the inlet and outlet coolant temperatures T_{in} and T_{out}, respectively:

$$T_{avg} = (T_{in} + T_{out}) / 2 \tag{3.1}$$

Rearrange the equation above, the limitation of the single lump model can be seen such that:

$$T_{out} = 2T_{avg} - T_{in} \tag{3.2}$$

Equation (3.2) shows that if the coolant inlet temperature suddenly increases, the outlet temperature will decrease at the same time, which is opposite to the reality.

The ordinary differential equations of Mann's model are derived below. The fuel temperature, T_F, is arrived at through a basic energy balance on the fuel lump:

$$\frac{dE_F}{dt} = \text{Heat generated in the fuel} - \text{Heat leaving the fuel} \tag{3.3}$$

where E_F is the heat energy in the fuel. Thus,

$$\frac{dE_F}{dt} = \frac{d(mcT)_F}{dt} = f \times P(t) - (UA)_{FC}(T_F - \theta_1) \tag{3.4}$$

where

m_F = the mass of the fuel,

c_F = the specific heat of the fuel,

f = the fraction of heat generated in the fuel,

$P(t)$ = the reactor power,

U_{FC} = the overall fuel-to-coolant heat transfer coefficient,

A_{FC} = the effective heat transfer surface area, and

θ_1 = the average temperature of the first coolant lump.

Equation (3.4) can be re-written as:

$$\frac{dT_F}{dt} = \frac{f}{(mc)_F} P(t) - \frac{1}{\tau_F}(T_F - \theta_1) \tag{3.5}$$

where $\tau_F = \frac{(mc)_F}{(UA)_{FC}}$ is the fuel heat transfer time constant.

Similarly, the differential equation for the first (inlet) coolant lump can be driven:

$$\frac{dE_{C1}}{dt} = \frac{d\left[(\frac{m}{2}c)_C \theta_1\right]}{dt} = \frac{(1-f)}{2} P(t) + (U\frac{A}{2})_{FC}(T_F - \theta_1) + (\dot{m}c)_C(\theta_{in} - \theta_1) \tag{3.6}$$

where

E_{C1} = the heat energy in the first (inlet) coolant lump,

m_C = the mass of the coolant,

c_C = the specific heat of the coolant,

$\dot{m}_C$ = the coolant mass flow rate, and

θ_{in} = the coolant inlet temperature.

Rearrange the equation above and get:

$$\frac{d\theta_1}{dt} = \frac{(1-f)}{(mc)_C} P(t) + \frac{1}{\tau_C}(T_F - \theta_1) - \frac{2}{\tau_R}(\theta_1 - \theta_{in}) \tag{3.7}$$

where $\tau_C = \frac{(mc)_C}{(UA)_{FC}}$ is the coolant heat transfer time constant and $\tau_R = \frac{m_C}{\dot{m}_C}$ is the coolant residence time in the core.

Thus, the differential equation for the second (outlet) coolant loop can be derived in the same way and get:

$$\frac{d\theta_2}{dt} = \frac{(1-f)}{(mc)_C} P(t) + \frac{1}{\tau_C}(T_F - \theta_1) - \frac{2}{\tau_R}(\theta_2 - \theta_1) \tag{3.8}$$

where θ_2 is the average temperature of the second coolant lump [15].

The matrix structure of the isolated core using Mann's model is shown below:

$$\mathbf{x} = \begin{bmatrix} \delta P \\ \delta C \\ \delta T_F \\ \delta \theta_1 \\ \delta \theta_2 \end{bmatrix} \quad \mathbf{A} = \begin{bmatrix} \frac{-\beta_T}{\Lambda} & \lambda & \frac{P_0 \alpha_F}{\Lambda} & \frac{P_0 \alpha_M}{2\Lambda} & \frac{P_0 \alpha_M}{2\Lambda} \\ \frac{\beta_T}{\Lambda} & -\lambda & 0 & 0 & 0 \\ \frac{f}{(mc)_F} & 0 & \frac{-1}{\tau_F} & \frac{1}{\tau_F} & 0 \\ \frac{(1-f)}{(mc)_C} & 0 & \frac{1}{\tau_C} & \frac{-1}{\tau_C} - \frac{2}{\tau_R} & 0 \\ \frac{(1-f)}{(mc)_C} & 0 & \frac{1}{\tau_C} & \frac{-1}{\tau_C} + \frac{2}{\tau_R} & \frac{-2}{\tau_R} \end{bmatrix} \quad \mathbf{f} = \begin{bmatrix} \frac{P_0 \delta \rho_{ext}}{\Lambda} \\ 0 \\ 0 \\ \frac{2\delta T_i}{\tau_R} \\ 0 \end{bmatrix} \tag{3.9}$$

Mann's model may also be implemented into a multi-lump reactor core with *N* fuel lumps and 2*N* coolant lumps. [16] The block diagram is shown as Figure 3.3.

Similar to the derivation of Equations (3.3) to (3.8), the differential equations of the multi-lump model can be derived:

$$\frac{dT_{F,i}}{dt} = \frac{f_i}{(\frac{m}{N}c)_F} P(t) - \frac{1}{\tau_{F,i}}(T_{F,i} - \theta_{2i-1}) \tag{3.10}$$

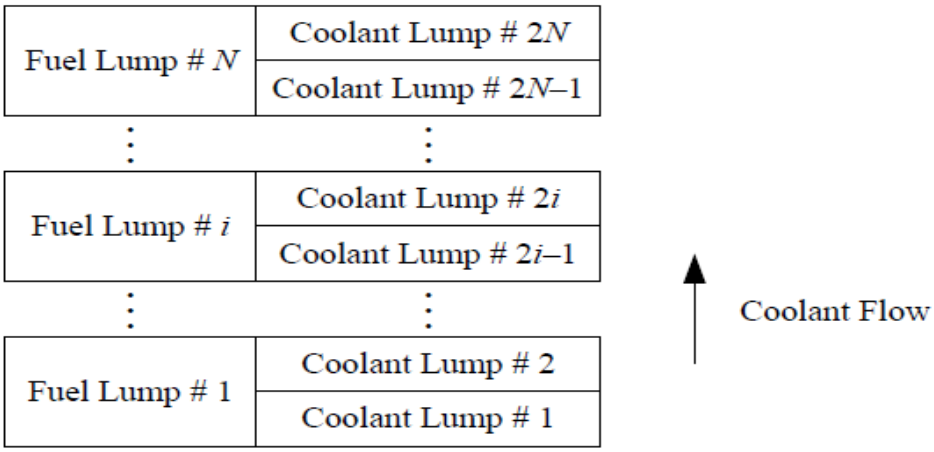

Fig. 3.3 Block diagram of Mann's model with multiple lumps.

For the odd ($j = 2i - 1$) coolant lumps:

$$\frac{d\theta_j}{dt} = \frac{f_j}{(\frac{m}{2N}c)_C} P(t) + \frac{1}{\tau_{C,i}}(T_{F,i} - \theta_j) - \frac{2}{\tau_R / N}(\theta_j - \theta_{j-1}) \tag{3.11}$$

For the even ($j = 2i$) coolant lumps:

$$\frac{d\theta_j}{dt} = \frac{f_j}{(\frac{m}{2N}c)_C} P(t) + \frac{1}{\tau_{C,i}}(T_{F,i} - \theta_{j-1}) - \frac{2}{\tau_R / N}(\theta_j - \theta_{j-1}) \tag{3.12}$$

Frequency Response

To get the frequency response, the matrix formulation is introduced, shown as:

$$\frac{d\mathbf{x}}{dt} = \mathbf{A}\mathbf{x}(t) + \mathbf{f} \tag{3.13}$$

where **x** is the input vector, **f** is the forcing functions vector, and **A** is the state matrix.

To solve for the frequency response, the equation above can be re-written as:

$$\frac{d\mathbf{x}}{dt} = \mathbf{A}\mathbf{x}(t) + \mathbf{b}y(t) \tag{3.14}$$

Then, take the Laplace transform of the entire set of equations and yield to:

$$s\mathbf{x}(s) - \mathbf{x}(0) = \mathbf{A}\mathbf{x}(s) + \mathbf{b}y(s) \tag{3.15}$$

$$\left[s\mathbf{I} - \mathbf{A}\right]\mathbf{x}(s) = \mathbf{b}y(s) \tag{3.16}$$

So, the transfer function can be written as:

$$\mathbf{G}(s) = \frac{\mathbf{x}(s)}{y(s)} = \left[s\mathbf{I} - \mathbf{A}\right]^{-1}\mathbf{b} \tag{3.17}$$

Substitute $s = j\omega$ into equation above and yield to:

$$\mathbf{G}(j\omega) = \left[j\omega\mathbf{I} - \mathbf{A}\right]^{-1}\mathbf{b} \tag{3.18}$$

Modeling and Simulation

In this thesis, a five fuel nodes and ten coolant nodes model has been utilized. The block diagram of this model is shown in Figure 3.4.

This model is simulated with MATLAB. The Bode plots of different transfer functions can be graphed to study their characteristics. There are two driven sources in this model, the change in reactivity $\delta\rho$ and the change in coolant inlet temperature $\delta\theta_{in}$, and three outputs, change in power δP, change in fuel temperature δT_F and change in coolant exit temperature $\delta\theta_{out}$. In order to study the characteristics of the model, only one driven source will be turned on at each

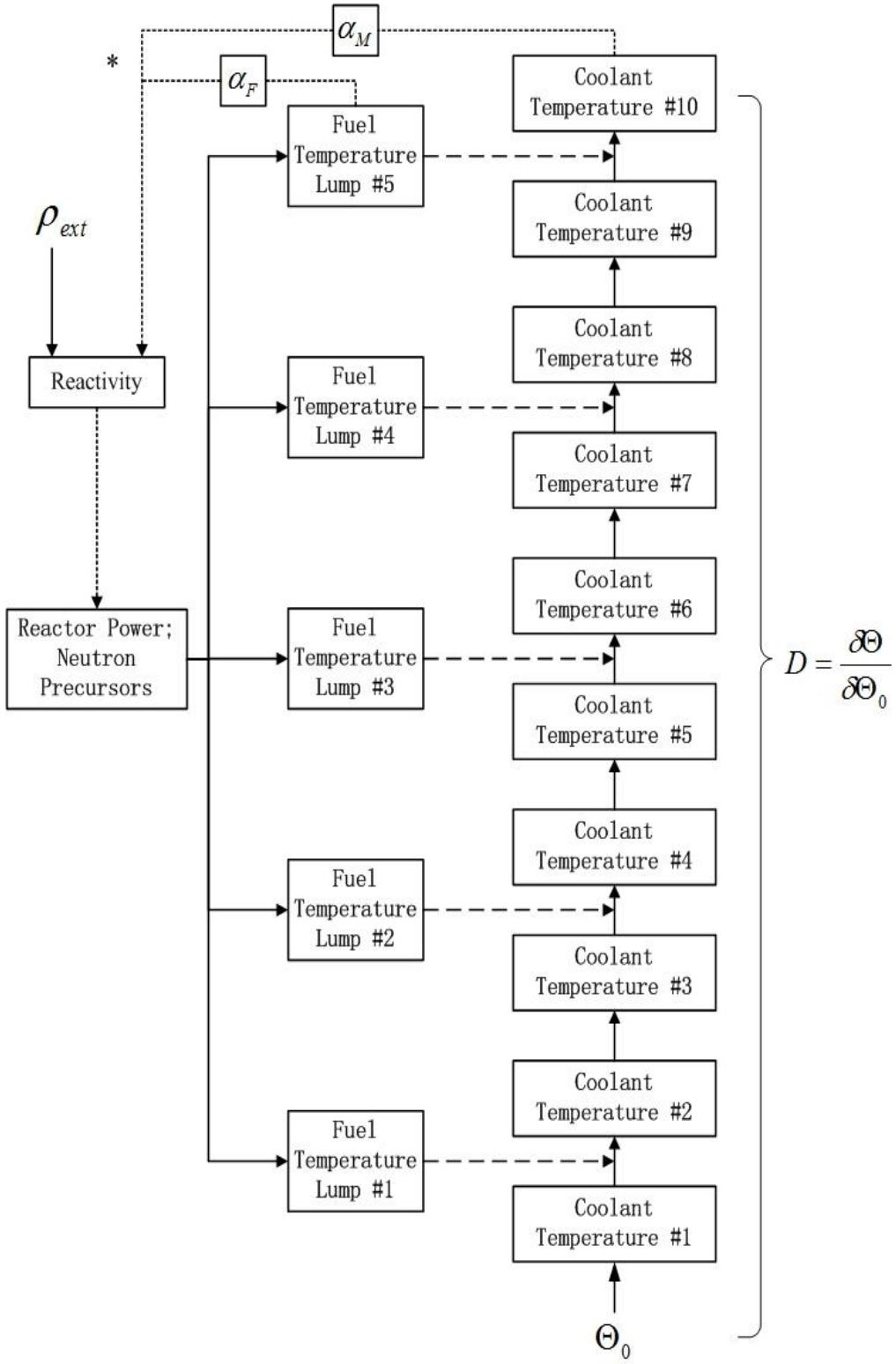

*Only one out of ten coolant and one out of five fuel feedback paths are shown.

Fig. 3.4 Multi fuel-coolant node model.

time and the other one will be set zero. All the data and parameters used in the model are from and based on the Palo Verde Nuclear Generating Station at Tonopah, Arizona [1] [2].

Reactivity Change as Input

First, the change in coolant inlet temperature is set to be zero. Thus, the transfer functions with a reactivity input change can be calculated and plotted. We shall find that the first five transfer functions presented have a break point at around 37.63 Hz. From the block diagram in Figure 3.4, it will be seen that all these five transfer functions share one part in common, that is the zero power transfer function introduced previously in Chapter II. Equation (2.14) shows that the zero power reactor transfer function has one zero at $\omega = \lambda$ and two poles at $\omega = 0$ and $\omega = \lambda + \frac{\beta}{\Lambda}$. Applying the data from this power plant finds the zero is at approximately 0.0152 Hz and the poles are at 0 Hz and around 37.63 Hz. This confirms that the pole of the zero power transfer function is the cause of this turning point.

The power to reactivity transfer function is plotted as in Figure 3.5. Compared to the plot of the zero power transfer function in Chapter V (Figure 5.2), the gain at the low frequency does not go to infinity. This is because of all the inherent reactivity feedback that bring the gain from infinity to a finite value.

This makes the reactor controllable at the low frequency which is important.

According to the rule of thumb that a one cent change in reactivity will cause one percent change in the power, this figure can be proved reasonable. From the MATLAB plot, the gain value of the plateau region can be read which is $5.23\times10^5\frac{MW}{\rho}$. Based on the theory, the change of power can be calculated as $1cent\times5.23\times10^5\frac{MW}{\rho}=(0.01\times0.0073)\rho\times5.23\times10^5\frac{MW}{\rho}=38.18MW$. The power of this reactor is 3800*MW*. Thus one percent of the power is $0.01\times3800MW=38MW$. They are not exactly the same but close enough for such an approximation.

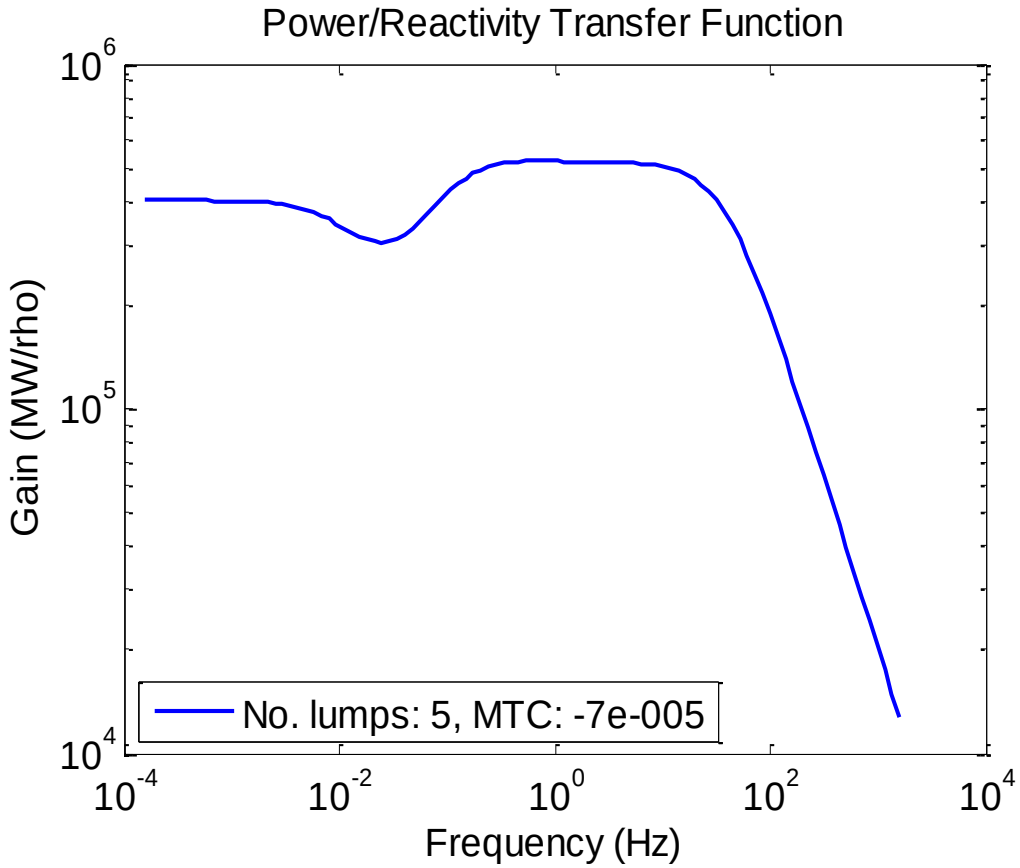

Fig. 3.5 Power to reactivity transfer function.

The fuel temperature at the upmost lump to reactivity transfer function is shown as Figure 3.6. There are three turning points at frequencies of 0.00572 Hz, 0.1484 Hz and 37.63 Hz. The curve comes in as a horizontal line until it hits the first break point and it decays one decade per four decades. Then it goes into the second break point and changes the slope to one decade per decade. Finally, it meets the third break point and the slopes changes to two decades per decade.

According to the definition of the fuel heat transfer time constant (τ_F), τ_F should have influence on the transfer function. All time constants and their corresponding frequencies ($f = \frac{1}{2\pi\tau}$) in this model are shown in Table 3.1. The parameters used to calculate the time constants are shown in Appendix A. Table 3.1 shows that this transfer function shold have a pole at 0.0487 Hz, however, it does not intially appear to.

In order to determine if there is error in this plot or not, some analysis is done to examine the plot. First, according to the characteristic of a pole in the Bode plot, if a pole occurs, the curve will go downward by one decade per decade. However, as stated before, after hitting the first break frequency, the curve did not decay one decade per decade. It decays one decade per four decades istead. That is saying that the first break point is not a pole. Using the insert line function and the data cursor function in MATLAB, the pole can be extrapolated, shown as Figure 3.7. First, draw a extension line of the horizontal line at the low frequency. Then, draw

the extension line of the curve between the second and third break frequency, which is decaying one decade per decade. Find the intersection of these two lines and draw a vertical line through that point. Use the data cursor function and find out that the pole is at 0.0551 Hz. This is close to the 0.0487 Hz which coresponds to the fuel heat transfer time constant. This proves that the plot is correct.

Since the plot is right, what caused the first and second break point? In Figure 3.4 it can be seen that there are two other mechanisms that may influence the plot. One is the fuel temperature coefficient of reactivity (α_F) and the other one is the moderator temperature coefficient of reactivity (α_M). A numerical experiment has been done in order to find out if this is the reason that caused the break frequencies. The experiment is done by changing only α_F and only α_M to zero, respectively. Then set both of them to zero. Compare these three plots with Figure 3.6 which none of them are zero. The result is shown as Figure 3.8. From the comparison it can be seen that α_F and α_M serve important roles to keep the core controllable. Otherwise, the value of this transfer function will go infinity at the low frequency. Also, it shows that it is the effect by both α_F and α_M that causes the first and the second break frequencies.

Table 3.1 Time constants and their corresponding frequencies

Time constant	Value [1]	Corresponding frequency
Fuel heat transfer time constant (τ_F)	3.265 sec	0.04875 Hz
Coolant heat transfer time constant (τ_C)	7.087 sec	0.02246 Hz
Coolant residence time in the core (τ_R)	0.7622 sec	0.2088 Hz

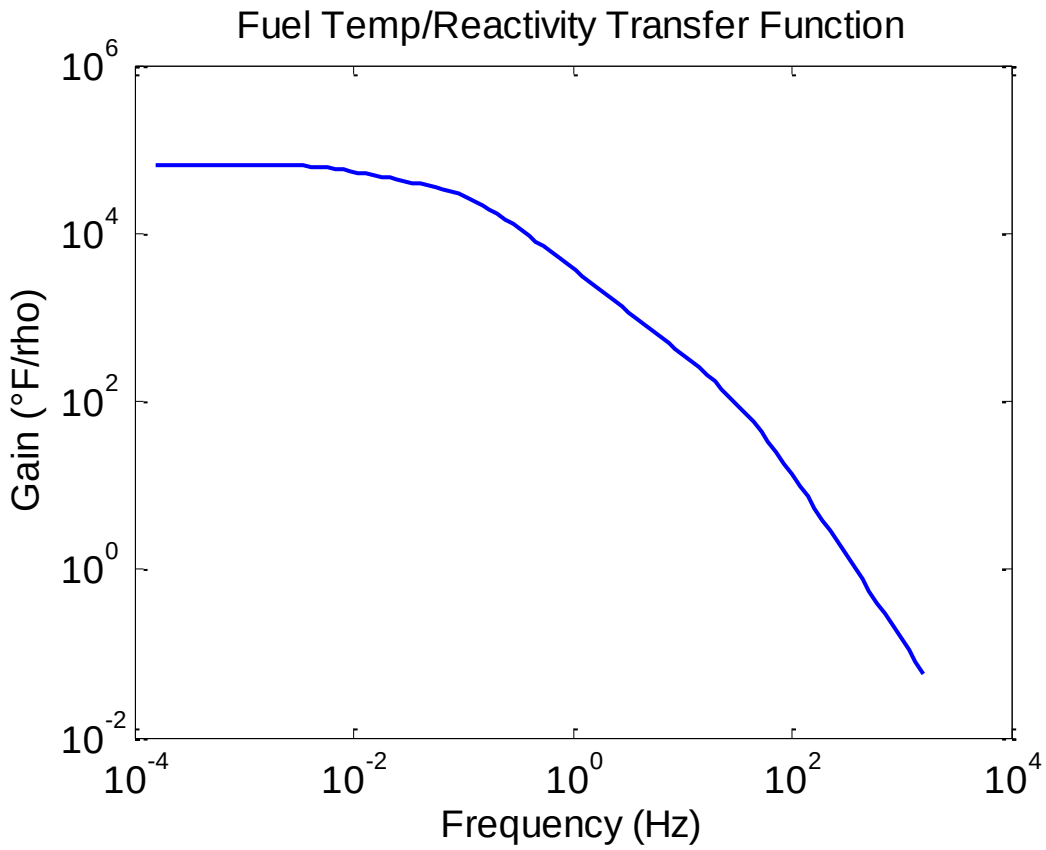

Fig. 3.6 Fuel temperature at the upmost lump to reactivity transfer function.

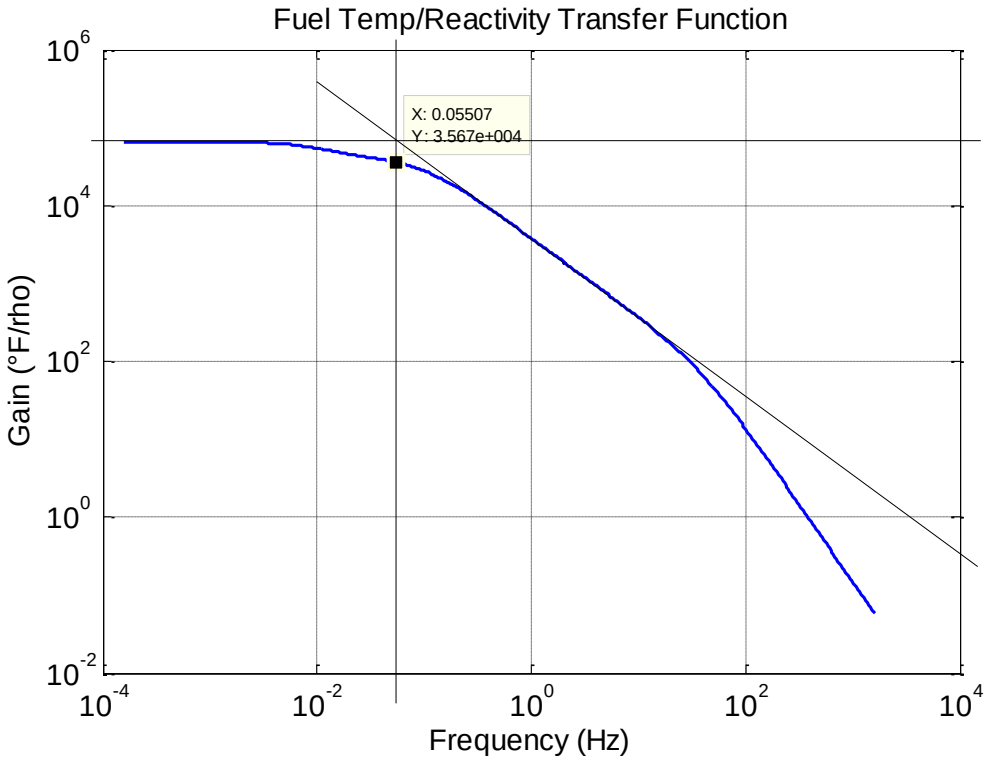

Fig. 3.7 Fuel temperature at the upmost lump to reactivity transfer function.

Figure 3.9 shows the transfer function of the coolant exit temperature to reactivity. The plot shows that it has a break frequency at 0.2056 Hz, which corresponds to $\tau = \frac{1}{2\pi f} = 0.7741\text{sec}$. It is very close to the value of coolant residence time in core τ_R which is 0.7622 sec. The low frequency behavior can be validated using a basic heat balance on the reactor, after a one cent increase in reactivity. From Figure 3.5, the gain at low frequency can be read using MATLAB, which is $4.019\times10^5 \frac{MW}{\rho}$. Then, the increase in power can be calculated as below:

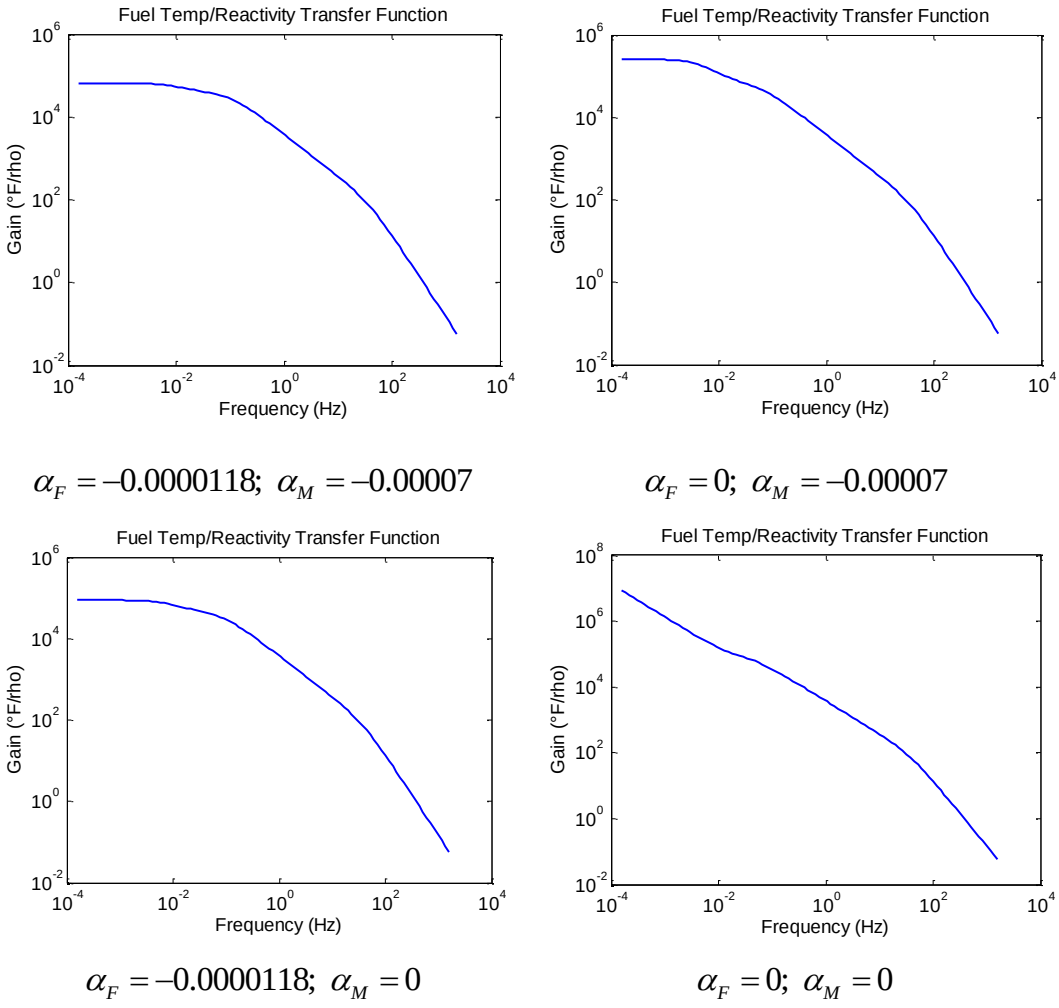

Fig. 3.8 Comparison of different α values.

$$\Delta P = 1cent \times 4.019 \times 10^5 \frac{MW}{\rho} = (0.01 \times 0.0073)\rho \times 4.019 \times 10^5 \frac{MW}{\rho} = 29.34MW \tag{3.19}$$

According to $\Delta P = \dot{m} c_p \Delta T$, the change in the coolant exit temperature can be computed as:

$$\Delta T = \frac{\Delta P}{\dot{m} c_p} = \frac{29.34MW}{\left(164 \times 10^6 \frac{lbm}{hr}\right)\left(1.4159 \frac{Btu}{lbm \cdot {}^\circ F}\right)\left(\frac{1kW \cdot hr}{3412Btu}\right)\left(\frac{1MW}{1000kW}\right)} = 0.431^\circ F \tag{3.20}$$

From MATLAB, the gain at the low frequency of Figure 3.9 can be read as $6606\frac{^\circ F}{\rho}$. Thus, the change in temperature for a one cent increase in reactivity should be $(0.01\times 0.0073)\rho\times 6606\frac{^\circ F}{\rho}=0.482^\circ F$. These two results match well.

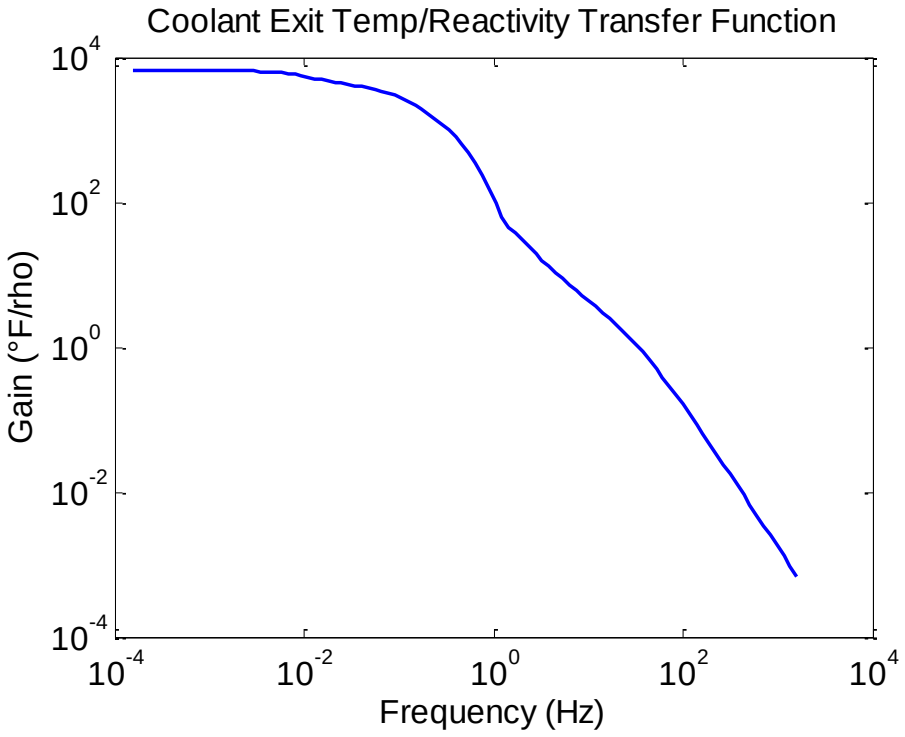

Fig. 3.9 Coolant exit temperature to reactivity transfer function.

According to the transfer functions above, more transfer functions can be easily derived. Figure 3.10 shows the coolant exit temperature to power transfer function. It has a turning point at 0.0210 Hz, which is $\tau=\frac{1}{2\pi f}=7.564\,\text{sec}$. From Table 3.1 can be seen that it is approximately same as the τ_C value, 7.0870 sec. The coolant temperature cannot keep up with power changes at high frequency because of heat transfer time delays.

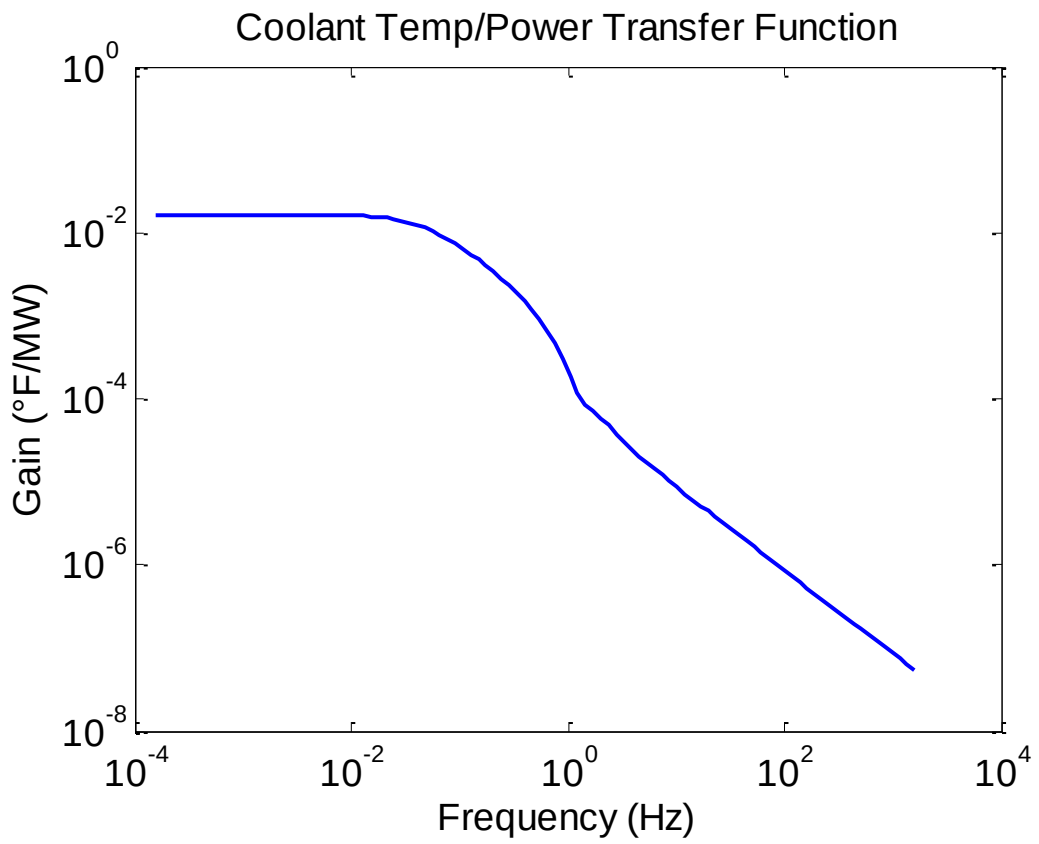

Fig. 3.10 Coolant exit temperature to power transfer function.

Figure 3.11 shows the transfer function of the coolant exit temperature to fuel temperature at the upmost lump. The gain at the low frequency is 0.1003 and it turns at 1.232 Hz. Similarly, coolant temperature changes at higher frequencies are constrained by time lags due to heat transfer.

Coolant Inlet Temperature Change as Input

Next, the change in reactivity is set to zero and coolant inlet temperature works as the driven source. Thus, the transfer functions of input $\delta\theta_{in}$ can be produced.

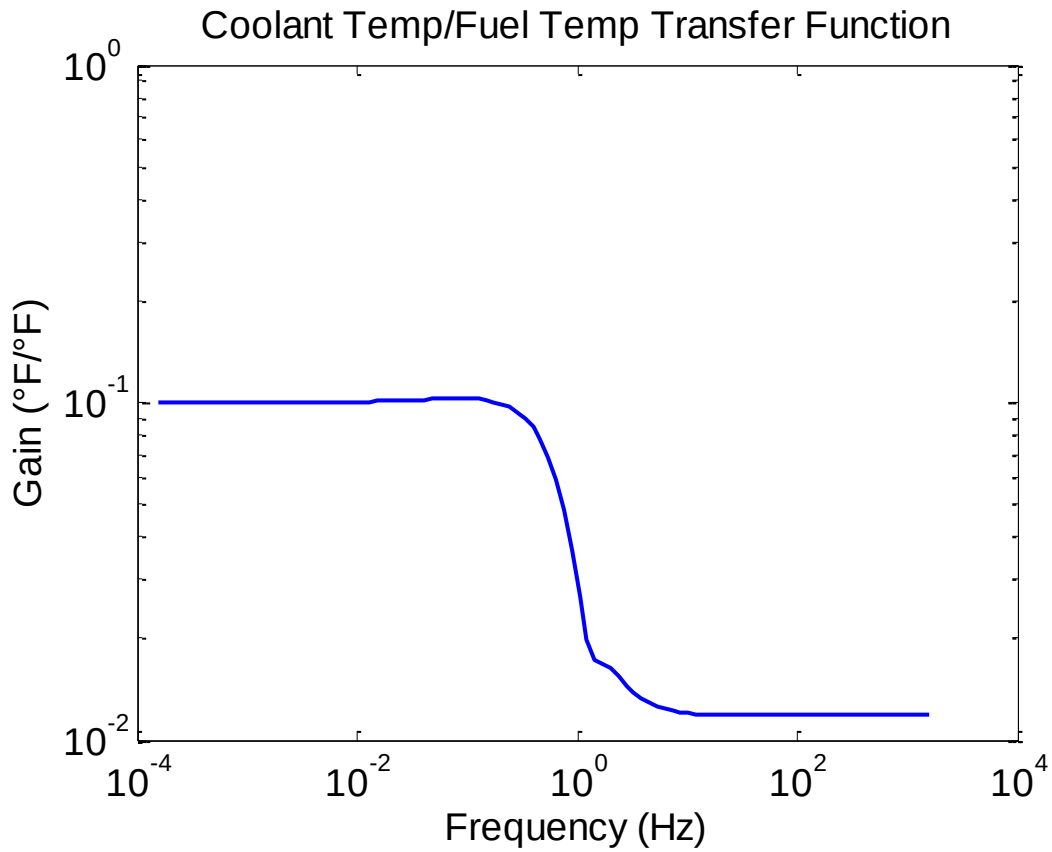

Fig. 3.11 Coolant exit temperature to fuel temperature at the upmost lump transfer function.

Figure 3.12 shows the transfer function between power and coolant inlet temperature. The same approach for the transfer function between fuel temperature and reactivity (Figure 3.7) is used here to obtain the pole of this transfer function. Use the insert line and data cursor function in MATLAB and find the pole is at 0.2056 Hz (shown in Figure 3.12), which is very close to the frequency of 0.209 Hz corresponding to the coolant residence time in the core (τ_R) (see Table 3.1).

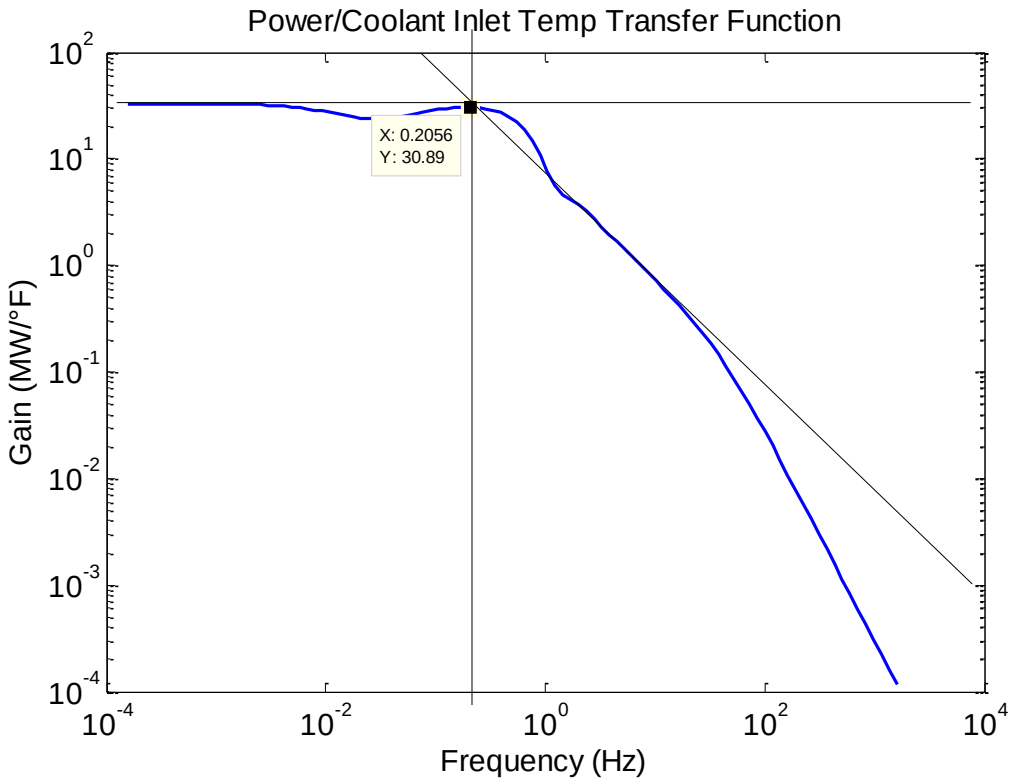

Fig. 3.12 Power to coolant inlet temperature transfer function.

The fuel temperature at the upmost lump to coolant inlet temperature transfer function is plotted as Figure 3.13. It shows a break point at 0.02419 Hz. From Table 3.1 it can be seen that this is caused by the coolant heat transfer time constant (τ_C) at 0.0225 Hz, which is reasonable.

Figure 3.14 is the coolant exit to inlet temperature transfer function. Using the same method for Figure 3.7, we find that the break frequency is 0.2056 Hz which is caused by the coolant residence time τ_R according to Table 3.1. The gain at the low frequency is slightly less than 1 which is reasonable because of the negative moderator reactivity feedback effect. However, the feature that the curve decays very fast after the break frequency requires a greater level of scrutiny.

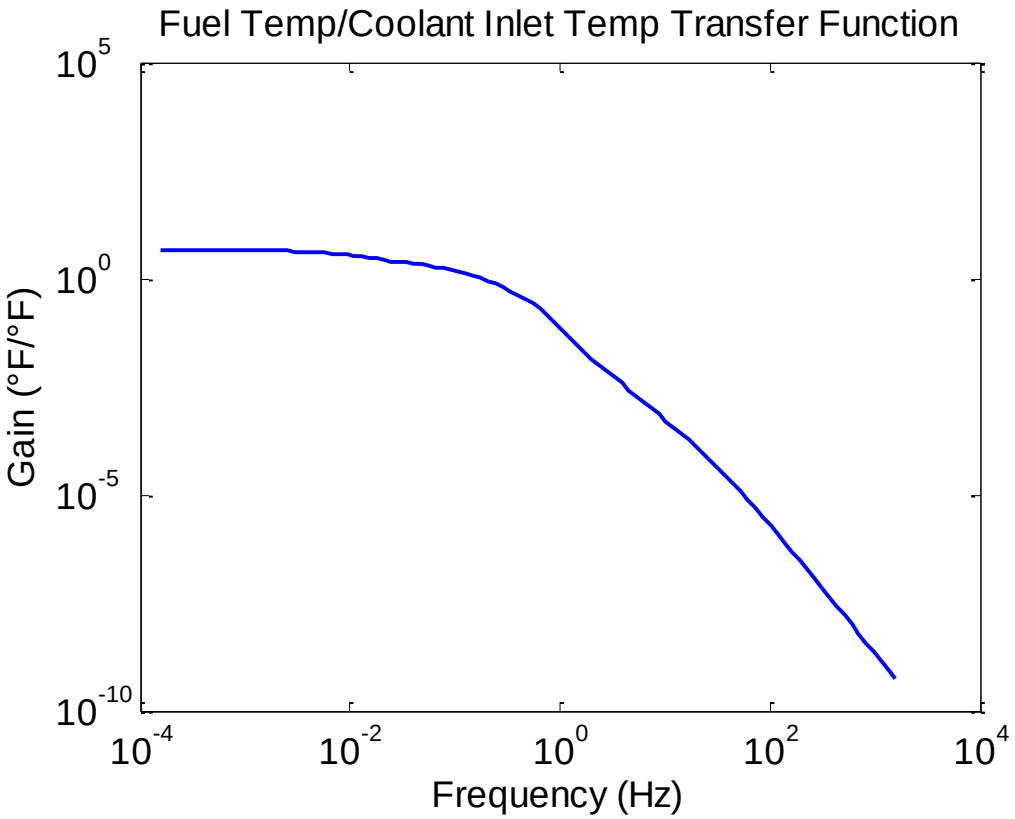

Fig. 3.13 Fuel temperature at the upmost lump to coolant inlet temperature transfer function.

Notice that the transfer function of each lump in the multi-lump model is not a pure time delay. It is a first-order transfer function in the form of $\frac{1}{1+s\tau}$. Therefore, this first-order transfer function has been compounded from the inlet to the lump which is specified. This causes the curve after the break frequency to become steeper with increasing numbers of lumps. In order to prove this, the transfer function between the even number coolant lumps (see Figure 3.4) and the coolant inlet temperature has been plotted, shown as Figure 3.15. It shows that along with the coolant lump goes higher and higher, the curve after the break frequency decays faster and faster. This proves that the conclusion is correct.

Another place that warrants attention is the gain at the low frequency. Figure 3.15 clearly shows that the gains at the low frequency are all slightly less than one, however, when the coolant lump goes higher, the gain becomes smaller. As mentioned before, the gain at low frequency is less than one because of the negative moderator reactivity feedback effect. This behavior here shows that the feedback is felt more and more moving up the core. This is because this transfer function includes not only the negative moderator reactivity feedback effect at one certain lump, but also the negative moderator reactivity feedback effects occurring before that location.

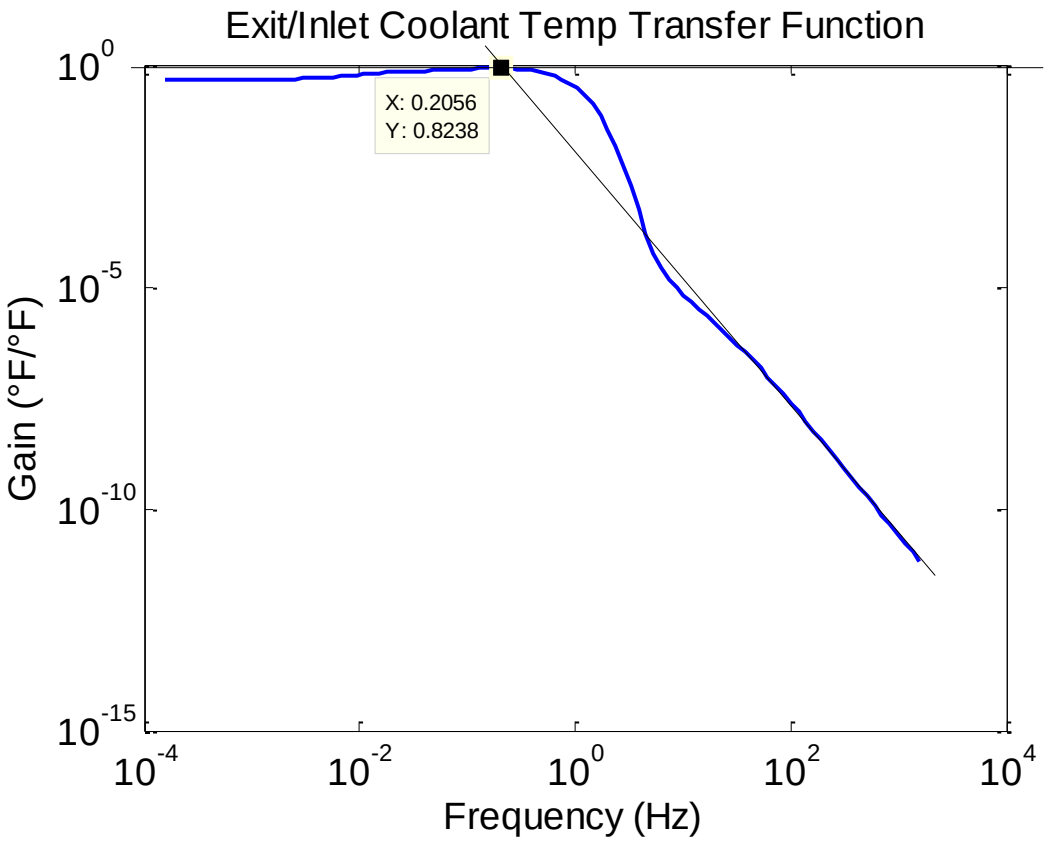

Fig. 3.14 Coolant exit to inlet temperature transfer function-reactivity.

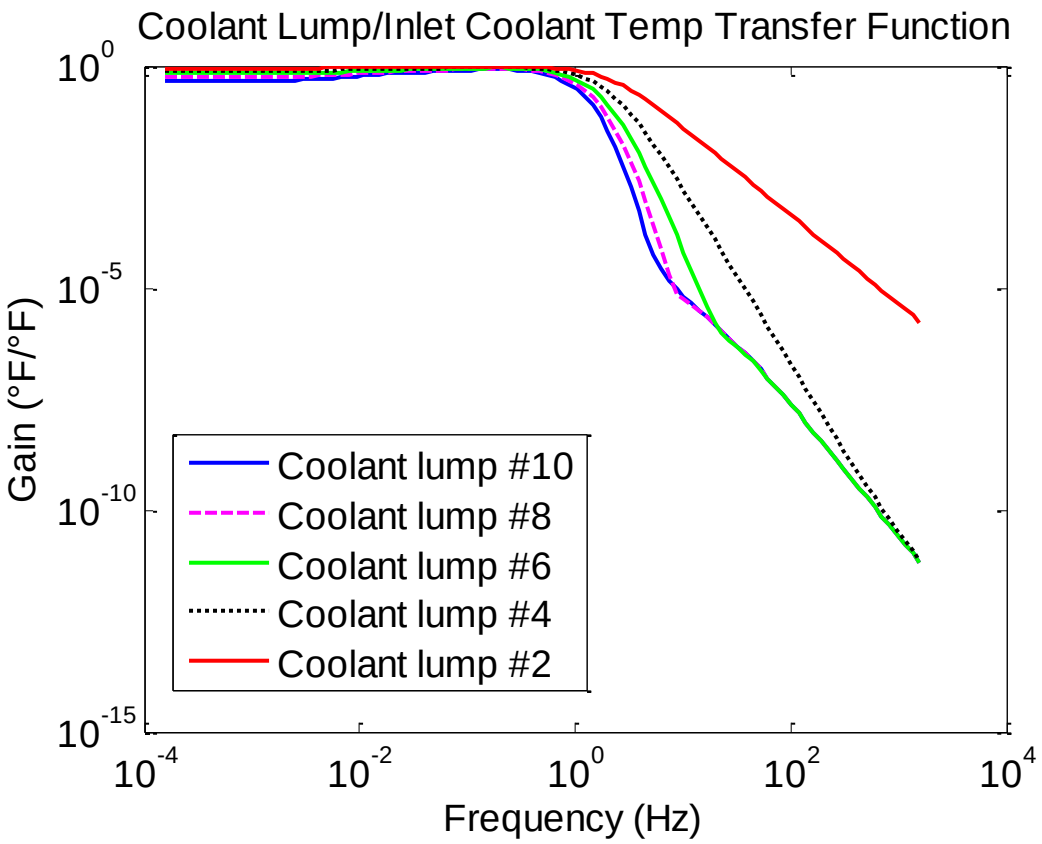

Fig. 3.15 Coolant lump temperature to coolant inlet temperature.

Fuel Temperature to Power Transfer Function in Both Cases

Figures 3.16 and 3.17 show the fuel temperature at the upmost lump to power transfer function when the driven source is change in reactivity and coolant inlet temperature, respectively. These two figures match pretty well. Figure 3.1 has a gain of 0.1638 at the low frequency while it is 0.1334 in Figure 3.14. Notice that both plots have a turning point at f = 0.0404 Hz, which corresponds to $\tau = \frac{1}{2\pi f} = 3.94\,\text{sec}$. It is very close to the τ_F value, 3.2650 sec shown in Table 3.1. Note that there is a slight difference between these two curves. This is because

that the transfer functions are not exactly same in each situation. From the Figure 3.3, it can be easily read that there is one more transfer function *D* when the coolant inlet temperature is the driven source rather than reactivity, which causes the difference between the plots.

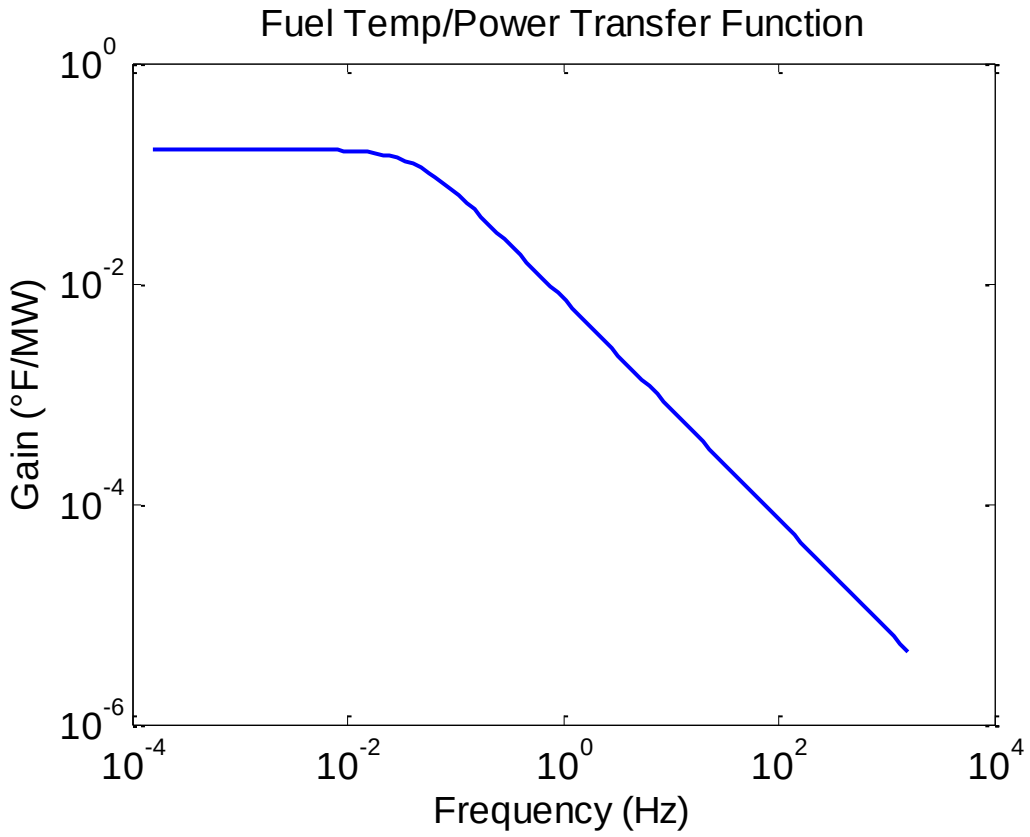

Fig. 3.16 Fuel temperature at the upmost lump to power transfer function-reactivity.

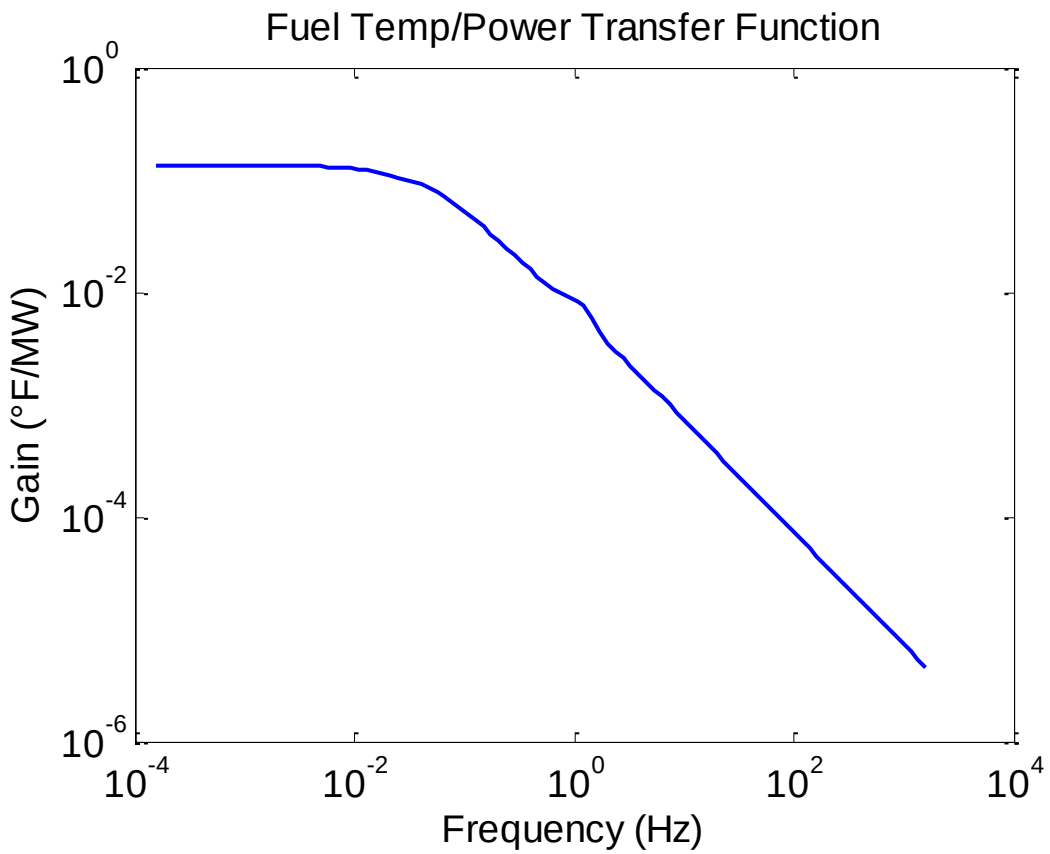

Fig. 3.17 Fuel temperature at the upmost lump to power transfer function-coolant inlet temperature.

CHAPTER IV

THEORY

Even though a lot of studies show that the multi-lump reactor core model using ordinary differential equations can be used to analyze the time dependent behavior of the nuclear power reactor, it cannot represent the changes in the spatially dependent variables during a transient situation which is important. Thus, the distributed-parameter model using partial differential equations is more advantageous in this situation. This chapter is going to present the general distributed parameter modeling theory, build a distributed parameter model for a PWR reactor and derive the transfer functions of that model.

General Distributed Method

The general equation of a distributed system is shown below:

$$L_r(\vec{r},t)z(\vec{r},t) = M_t(\vec{r},t)z(\vec{r},t) + C(\vec{r},t) \tag{4.1}$$

where

$\vec{r}$ = position vector,

L_r = a linear differential operator containing all derivatives with respect to position and all constants,

z = the position and time dependent output variable,

M_t = a linear differential operator containing all derivatives with respect to

time,

$C(\vec{r},t)$ = a forcing function (inhomogeneous term).

It takes two steps to obtain the solution in the frequency domain:

1. Laplace transform the expression with respect to time, which gives:

$$L_r(\vec{r},s)z(\vec{r},s) = M_s(\vec{r},s)z(\vec{r},s) + C(\vec{r},s) \tag{4.2}$$

where the zero initial conditions have been imposed.

2. Solve the space dependent equation above by separation of variables for $z(\vec{r},s)$. Use proper boundary conditions to couple the system to other parts of the system and the external conditions.

Distributed-Parameter Model of PWR

The model which is going to be built could be shown as that in Figure 4.1.

Now, the transfer functions for the heat transfer in the pressurized water reactor (PWR) core can be developed by the method above. Some assumptions are made to reach the result:

1. The heat transfer is one-dimensional with uniform heat generation throughout the reactor core,
2. The heat generated is transferred to a flowing coolant.

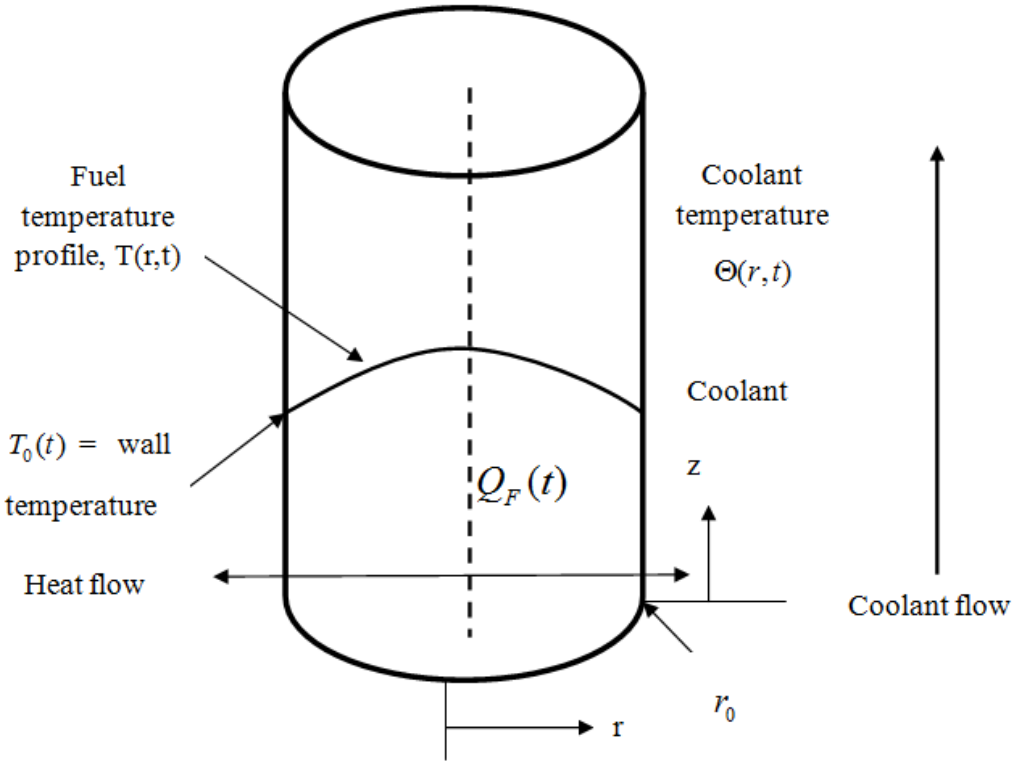

Fig. 4.1 Distributed-parameter model of a PWR.

Fuel Rod Temperature

The partial differential equation that describes the heat production and heat transfer through the fuel rod is: [17]

$$\frac{1}{r^2}\frac{\partial}{\partial r}\left(r^2\frac{\partial T}{\partial r}\right)=\frac{-Q_F(t)}{k}+\frac{\rho_F c_{pF}}{k}\frac{\partial T}{\partial t} \tag{4.3}$$

where

Q_F = heat generation rate per unit volume in the fuel rod,

k = thermal conductivity of the fuel rod,

ρ_F = fuel density,

c_{pF} = specific heat of the fuel,

The boundary conditions are:

$$\frac{\partial T}{\partial r} = 0 \quad \text{at} \quad r = 0 \quad \text{(the fuel rod centerline)} \tag{4.4}$$

$$k\frac{\partial T}{\partial r} = -h\left(T_0 - \Theta\right) \quad \text{at} \quad r = r_0 \quad \text{(Newton's law of cooling at fuel surface)} \tag{4.5}$$

where

T_0 = temperature in the material at $r = r_0$,

Θ = temperature of the coolant fluid,

h = surface heat transfer coefficient,

r_0 = radius of the cylindrical fuel rod.

According to the method of the distributed system, the first step is to Laplace transform the partial differential Equation (4.3) and get:

$$\frac{1}{r^2}\frac{\partial}{\partial r}(r^2\frac{\partial T(r,s)}{\partial r}) = \frac{-Q_F(s)}{k} + \alpha^2 T(r,s) \tag{4.6}$$

where $\alpha^2 = \frac{\rho_F c_{pF} s}{k}$. The general form of the solution is:

$$T(r,s) = \frac{Q_F(s)}{\rho_F c_{pF} s} + AI_0(\alpha r) + BK_0(\alpha r) \tag{4.7}$$

where I_0 is the modified Bessel functions of the first kind of order zero and K_0 is the modified Bessel functions of the second kind of order zero.

To solve for the constant coefficients *A* and *B*, the derivative of the solution is taken and get:

$$\frac{\partial T(r,s)}{\partial r} = A\alpha I_1(\alpha r) - B\alpha K_1(\alpha r) \tag{4.8}$$

where I_1 and K_1 are the modified Bessel functions of the first and second kind of order one, respectively.

Here, the boundary conditions are applied. Employing Equation (4.4) yields:

$$\left.\frac{\partial T(r,s)}{\partial r}\right|_{r=0} = 0 = A\alpha I_1(0) - B\alpha K_1(0) = A\alpha \times 0 - B\alpha \times \infty \tag{4.9}$$

Thus, $B = 0$ and the solution can be written as:

$$T(r,s) = \frac{Q_F(s)}{\rho_F c_{pF} s} + AI_0(\alpha r) \tag{4.10}$$

Next, Equation (4.15) is applied:

$$k\left.\frac{\partial T(r,s)}{\partial r}\right|_{r=r_0} = -h\left[T_0(s) - \Theta(s)\right] \tag{4.11}$$

Substituting Equation (4.10) to (4.11) and yields:

$$k\alpha AI_1(\alpha r_0) = -\frac{hQ_F(s)}{\rho_F c_{pF} s} - hAI_0(\alpha r_0) + h\Theta(s) \tag{4.12}$$

Then, the constant coefficient *A* can be solved:

$$A = \frac{-\dfrac{hQ_F(s)}{\rho_F c_{pF} s} + h\Theta(s)}{k\alpha I_1(\alpha r_0) + hI_0(\alpha r_0)} \tag{4.13}$$

Now, put *A* into Equation (4.10). The solution can be written as:

$$T(r,s) = \frac{Q_F(s)}{\rho_F c_{pF} s} + \frac{-\dfrac{hQ_F(s)}{\rho_F c_{pF} s} + h\Theta(s)}{k\alpha I_1(\alpha r_0) + hI_0(\alpha r_0)} I_0(\alpha r) \tag{4.14}$$

or equivalently:

$$T(r,s)=\frac{Q_F(s)}{\rho_F c_{pF} s}\left[1-\frac{hI_0(\alpha r)}{k\alpha I_1(\alpha r_0)+hI_0(\alpha r_0)}\right]+\Theta(s)\left[\frac{hI_0(\alpha r)}{k\alpha I_1(\alpha r_0)+hI_0(\alpha r_0)}\right] \quad (4.15)$$

Therefore, two transfer functions can be determined from the equation above:

$$\frac{T(r,s)}{Q_F(s)}=\frac{1}{\rho_F c_{pF} s}\left[1-\frac{hI_0(\alpha r)}{k\alpha I_1(\alpha r_0)+hI_0(\alpha r_0)}\right] \quad (4.16)$$

and

$$\frac{T(r,s)}{\Theta(s)}=\frac{hI_0(\alpha r)}{k\alpha I_1(\alpha r_0)+hI_0(\alpha r_0)} \quad (4.17)$$

The former transfer function describes how the fuel temperature varies with heat generation (fission) changes, whereas the latter transfer function shows the change in fuel temperature with coolant temperature.

Coolant Temperature and Flow

Another equation needed to establish the core heat transfer model is the heat balance for the coolant. Here, some assumptions are made:

1. The coolant density ρ_c is constant. Thus the mass is constant;
2. The flow is constant. Therefore, the momentum balance is not needed.
3. The coolant and moderator are incompressible media. Most nuclear power reactors use water, which is incompressible, as both the coolant and moderator.
4. The heat generated from the fuel rod is directly transferred to the coolant (i.e. the gap and cladding are ignored).

Then, the convection heat transfer between the fuel rod and the coolant (single-phase, incompressible, one-dimensional slug flow) can be described by the partial differential equation below:

$$\frac{\partial \Theta}{\partial t} + u\frac{\partial \Theta}{\partial z} = \frac{hP}{A\rho_c c_{pc}}(T_0 - \Theta) + \frac{Q_c(t)}{\rho_c c_{pc}} \tag{4.18}$$

where

ρ_c = coolant density,

c_{pc} = specific heat of the coolant,

Q_C = volumetric heat generation in coolant,

z = axial height (distance from core base),

$u = \frac{\dot{m}}{\rho A}$ = coolant velocity,

$\dot{m}$ = mass flow rate,

P = heated perimeter of the coolant channel,

A = cross-sectional flow area of the channel.

Then, take the Laplace transform of the equation above,

$$s\Theta(z,s) + u\frac{\partial \Theta(z,s)}{\partial z} = b[T_0(s) - \Theta(z,s)] + \frac{Q_C(s)}{\rho_c c_{pc}} \tag{4.19}$$

where $b = \frac{hP}{A\rho_c c_{pc}}$.

From Equation (4.15) derived earlier, the wall temperature T_0 in terms of the fluid temperature can be determined:

$$T_0(s) = \frac{Q_F(s)}{\rho_F c_{pF} s}\left[1 - \frac{hI_0(\alpha r_0)}{k\alpha I_1(\alpha r_0) + hI_0(\alpha r_0)}\right] + \Theta(s)\left[\frac{hI_0(\alpha r_0)}{k\alpha I_1(\alpha r_0) + hI_0(\alpha r_0)}\right] \tag{4.20}$$

Substitute the equation above into Equation (4.24) and get:

$$\begin{aligned} s\Theta(z,s) + u\frac{\partial\Theta(z,s)}{\partial z} &= \frac{bQ_F(s)}{(\rho c_p)_F s}\left[1 - \frac{hI_0(\alpha r_0)}{k\alpha I_1(\alpha r_0) + hI_0(\alpha r_0)}\right] \\ &+ b\Theta(z,s)\left[\frac{hI_0(\alpha r_0)}{k\alpha I_1(\alpha r_0) + hI_0(\alpha r_0)} - 1\right] + \frac{Q_C(s)}{(\rho c_p)_C} \end{aligned} \tag{4.21}$$

or equivalently:

$$\frac{\partial\Theta(z,s)}{\partial z} + \frac{s - bR}{u}\Theta(z,s) = \frac{Q_C(s)}{u(\rho c_p)_C} - \frac{bRQ_F(s)}{u(\rho c_p)_F s} \tag{4.22}$$

where

$$R = \frac{I_0(\alpha r_0)}{\frac{k\alpha}{h} I_1(\alpha r_0) + I_0(\alpha r_0)} - 1 \tag{4.23}$$

The solution of the equation is:

$$\Theta(z,s) = \Theta_0(s)e^{-\frac{(s-bR)z}{u}} + \left[\frac{Q_C(s)}{(\rho c_p)_C} - \frac{bRQ_F(s)}{(\rho c_p)_F s}\right]\left(\frac{1}{s - bR}\right)\left[1 - e^{-\frac{(s-bR)z}{u}}\right] \tag{4.24}$$

From the solution, three transfer functions can be obtained:

$$\frac{\Theta(z,s)}{\Theta_0(s)} = \frac{\Theta(z,s)}{\Theta(0,s)} = e^{-\frac{(s-bR)z}{u}} \tag{4.25}$$

$$\frac{\Theta(z,s)}{Q_C(s)} = \frac{1 - e^{-\frac{(s-bR)z}{u}}}{(\rho c_p)_C(s - bR)} \tag{4.26}$$

$$\frac{\Theta(z,s)}{Q_F(s)} = \frac{-bR}{(\rho c_p)_F s(s - bR)}\left[1 - e^{-\frac{(s-bR)z}{u}}\right] \tag{4.27}$$

Combined Fuel and Coolant

Then, the model of the heat conduction of the fuel and the model of the convection to the coolant can be combined to establish the full distributed parameter model of a PWR. Therefore, several transfer functions are obtained:

$$\frac{\delta T(r,z,s)}{\delta \Theta(0,s)} = \frac{\text{change in fuel temperature at the height } z \text{ and radius } r}{\text{change in the coolant inlet } (z=0) \text{ temperature}} = \frac{\delta T(r,s)}{\delta \Theta(s)} \frac{\delta \Theta(z,s)}{\delta \Theta(0,s)} \tag{4.28}$$

$$\frac{\delta T(r,z,s)}{\delta Q_F(s)} = \frac{\text{change in fuel temperature at the height } z \text{ and radius } r}{\text{change in the fuel heat source output}} = \frac{\delta T(r,s)}{\delta \Theta(s)} \frac{\delta \Theta(z,s)}{\delta Q_F(s)} + \frac{\delta T(r,s)}{\delta Q_F(s)} \tag{4.29}$$

$$\frac{\delta T(r,z,s)}{\delta Q_C(s)} = \frac{\text{change in fuel temperature at the height } z \text{ and radius } r}{\text{change in the coolant heat source output}} = \frac{\delta T(r,s)}{\delta \Theta(s)} \frac{\delta \Theta(z,s)}{\delta Q_C(s)} \tag{4.30}$$

$$\frac{\delta \Theta(z,s)}{\delta \Theta(0,s)} = \frac{\text{change in coolant temperature at the axial position } z}{\text{change in the coolant inlet temperature}} \tag{4.31}$$

$$\frac{\delta \Theta(z,s)}{\delta Q_F(s)} = \frac{\text{change in coolant temperature at the axial position } z}{\text{change in the fuel heat source output}} \tag{4.32}$$

$$\frac{\delta \Theta(z,s)}{\delta Q_C(s)} = \frac{\text{change in coolant temperature at the axial position } z}{\text{change in the coolant heat source output}} \tag{4.33}$$

In order to have a better physical understanding of the equations derived above, Figure 4.2 is made to show the relationship of the variables and the transfer functions between two different variables. For example, Equation 4.16 is the transfer function from the fuel heat generation to the fuel temperature and Equation 4.17 shows the transfer function between the fuel temperature and the

coolant temperature; while Equation 4.15 combines both transfer functions whereas Equation 4.27 also includes coolant flow up the reactor.

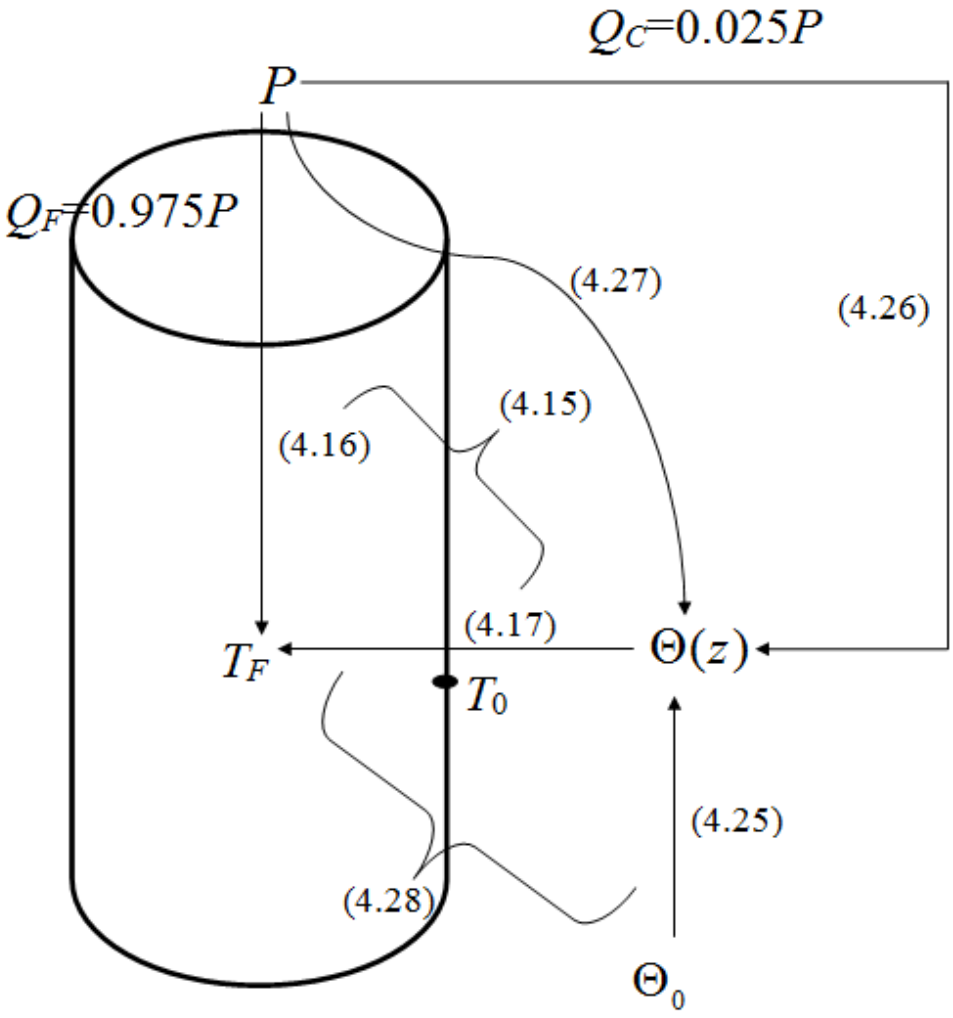

Fig. 4.2 Transfer functions between variables where the number in brackets refers to the equation number derived in the text.

CHAPTER V

MODELING AND SIMULATION

For safety purposes, commercial nuclear power plants nowadays rarely accept any experiments or any test equipment attached to the reactor except those necessary to carry out required operations. Thus, creating a model of the nuclear reactor is necessary for simulation studies.

Modeling

Since the majority of nuclear power plants use Pressurized Water Reactors (PWR), the model that is built up here is a PWR for the simulation and studies. To get a more accurate result, a distributed-parameter model is constructed. In order to have a better understanding, the overall block diagram of the PWR distributed parameter model has been made as Figure 5.1. For comparison, the results of the multi fuel-coolant node model employed in Chapter III will be used. Note that there are some slight differences between the gain of the transfer functions for the distributed model and the multi-lump model. It is because for the distributed parameter model, the fuel-to-coolant heat transfer is isolated at a certain height. The core averaged effects and feedback at other places are not explicitly included is the transfer function. However, the multi-lump model cannot be isolated at a certain level. It is an integral and average value for the core. Thus, all the effects

and feedbacks have been added to its transfer functions. All data and parameters used in the model are from and based on the Palo Verde Nuclear Generating Station at Tonopah, Arizona [1] [2].

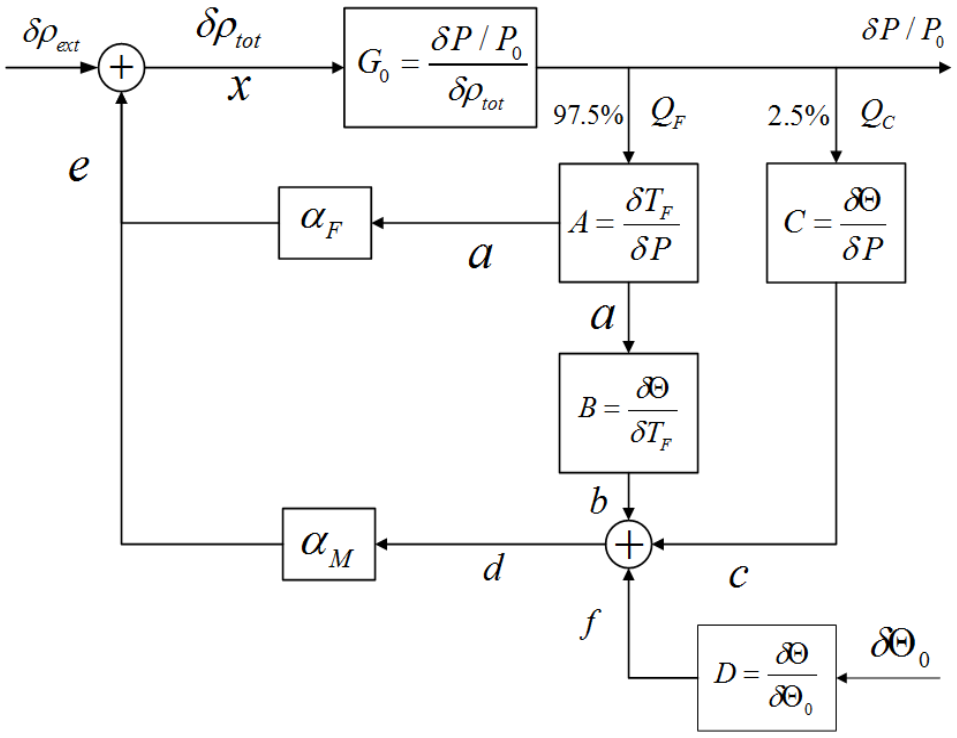

Fig. 5.1 The overall block diagram of the PWR distributed parameter model.

From the block diagram, the overall transfer function of the change in power to the change in the reactivity $\frac{\delta P / P_0}{\delta\rho_{tot}}$ can be derived as follows:

$$a = xG_0A \tag{5.1}$$

$$b = aB = xG_0AB \tag{5.2}$$

$$c = xG_0C \tag{5.3}$$

$$f = D\delta\Theta_0 \tag{5.4}$$

$$d = b + c + f = xG_0AB + xG_0C + D\delta\Theta_0 = xG_0(AB + C) + D\delta\Theta_0 \tag{5.5}$$

$$e = \alpha_F a + \alpha_M d = \alpha_F xG_0A + \alpha_M xG_0(AB + C) + \alpha_M D\delta\Theta_0 \tag{5.6}$$

$$x = \delta\rho_{ext} + e \tag{5.7}$$

Since this is a double-input single-output system, two transfer functions can be obtained by setting each input to zero separately:

(1) If $\delta\Theta_0 = 0$, then the output due to a reactivity change is

$$F(s) = \frac{\delta P / P_0}{\delta\rho_{ext}} = \frac{xG_0}{x - e} = \frac{G_0}{1 - \left[\alpha_F G_0 A + \alpha_M G_0(AB + C)\right]} \tag{5.8}$$

(2) If $\delta\rho_{ext} = 0$, then the output due to a core inlet coolant temperature change is

$$H(s) = \frac{\delta P / P_0}{\delta\Theta_0} = \frac{xG_0}{\dfrac{x - \alpha_F a}{\alpha_M} - b - c \over D} = \frac{\alpha_M DG_0}{1 - \left[\alpha_F G_0 A + \alpha_M G_0(AB + C)\right]} \tag{5.9}$$

Simulation

Individual Transfer Functions

In Equations (5.8) and (5.9), the zero power transfer function G_0 (introduced in Chapter II) is a basic and important transfer function. Recall that the zero power transfer function can be calculated as:

$$G_0(\omega) = \frac{\delta P(\omega) / P_0}{\delta\rho(\omega)} = \frac{j\omega + \lambda}{j\omega\Lambda(j\omega + \lambda + \dfrac{\beta}{\Lambda})} \tag{5.10}$$

where

P_0 = the steady-state power generated in core,

λ = delayed neutron precursor decay constant,

Λ = neutron generation time, and

β = delayed neutron fraction.

Using MATLAB, the frequency domain response of the zero power transfer function is plotted in Figure 5.2. The graph shows that the transfer function has a zero at approximately 0.01519 Hz and two poles at 0 Hz and around 37.63 Hz which agrees with the theory that the zero power transfer function has a zero at λ and two poles at 0 and $\lambda + \frac{\beta}{\Lambda}$.

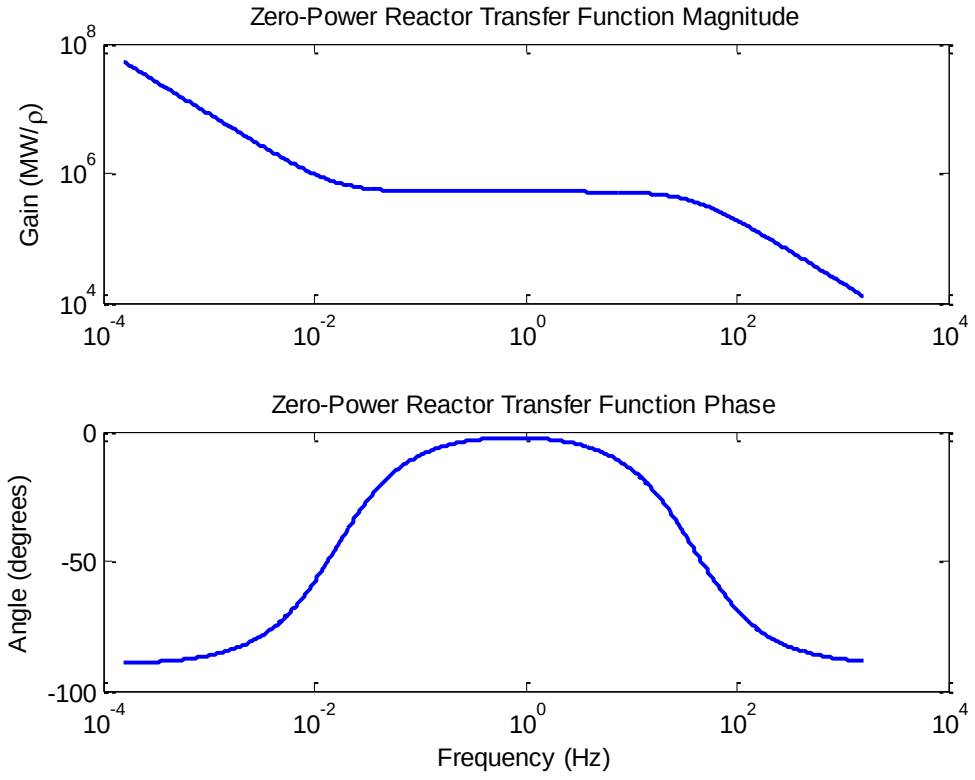

Fig. 5.2 Zero-power reactor transfer function.

From Figure 5.1, *A* is the transfer function of fuel temperature to power. It has been derived in Chapter IV and shown as Equation (4.29). It can be calculated and plotted as Figure 5.3. It shows that the fuel temperature response is the same at different heights. It is reasonable because the heat source in this model is assumed to produce heat uniformly along the fuel rod. Without this assumption, the fuel temperature will be different at different heights. Compare it to the plot of the multi-lump model Figure 5.4, the gain at low frequency of Figure 5.3 and 5.4 are 0.1795 and 0.1638, respectively. The break frequencies are both 0.0404 Hz, which corresponds to the fuel heat transfer time constant (τ_F) shown in Table 3.1. Then, it decays one decade per decade. These two plots agree very well.

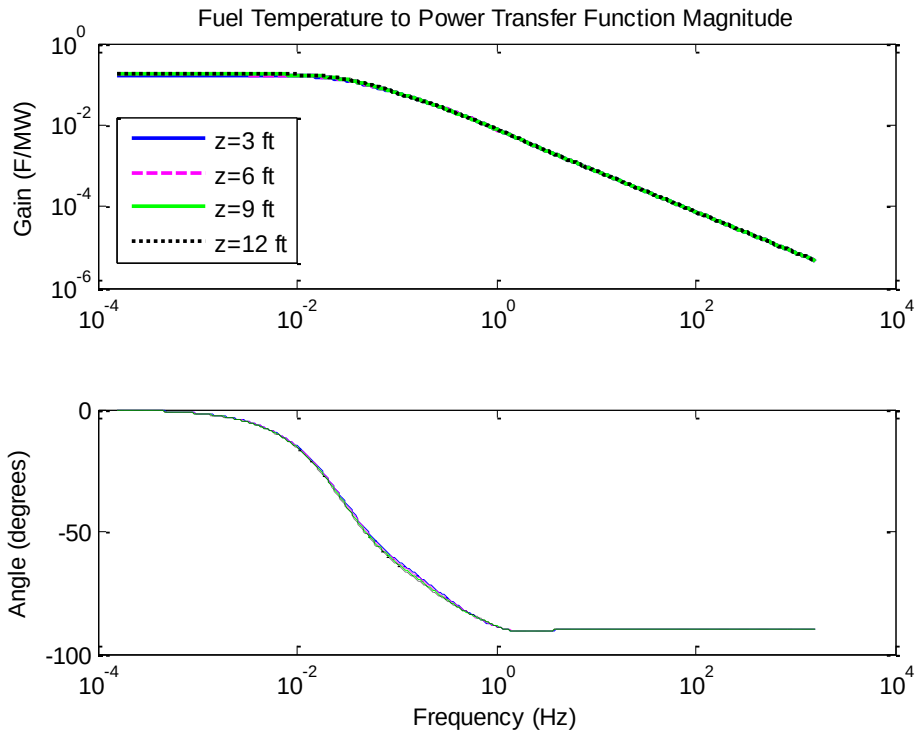

Fig. 5.3 Fuel temperature to power transfer function - distributed-parameter.

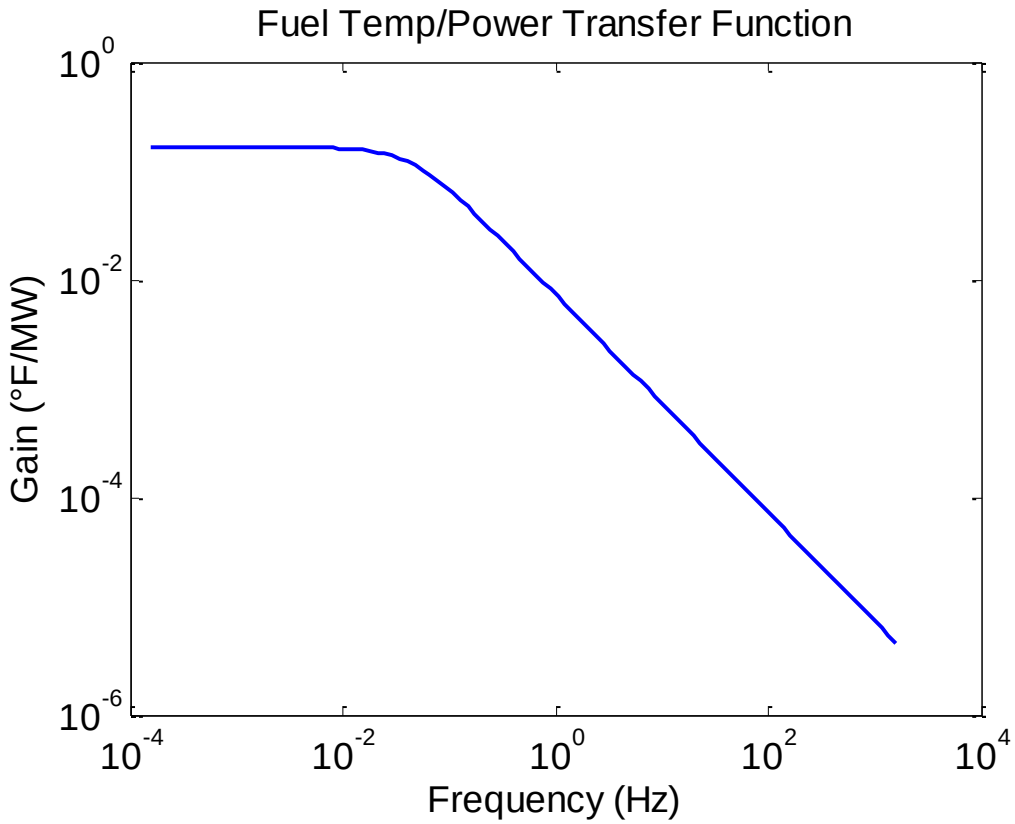

Fig. 5.4 Fuel temperature to power transfer function – multi node.

Equation (4.32) shows the transfer function of coolant temperature to the fuel heat production $\frac{\Theta(z,s)}{Q_F(s)}$ (Equation 4.27) which is the product of *A* and *B* in Figure 5.1. It has been plotted and shown in Figure 5.5. The gain at the low frequency at the coolant exit is 0.1561. It has a break frequency at 0.0223 Hz. From Table 3.1, it shows that this is caused by the coolant heat transfer time constant (τ_C), which is reasonable. This means that if the fuel heat production changes faster than τ_C, then the coolant temperature will not be able to keep up with the change.

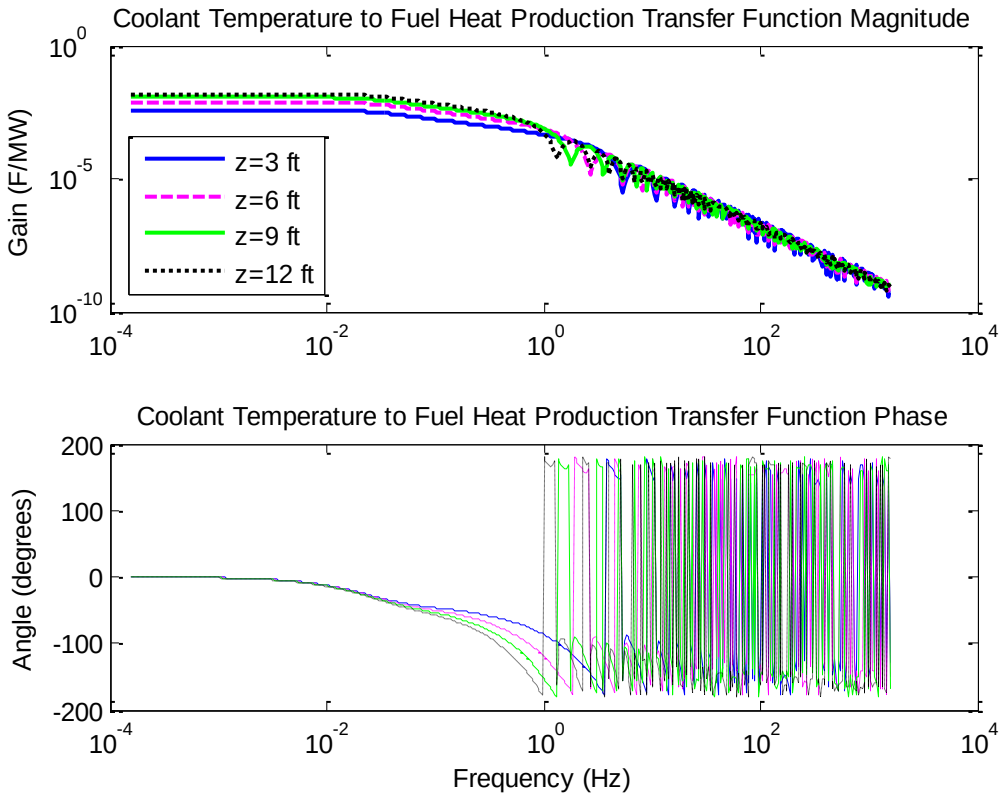

Fig. 5.5 Coolant temperature to fuel heat production transfer function.

With those two transfer functions plotted above, the transfer function *B* in Figure 5.1 can be calculated by dividing the transfer function of coolant temperature to the fuel heat production (*A* times *B*) by the transfer function of fuel temperature to power (*A*), shown in Figure 5.6. However, it is only one part of the transfer function of coolant temperature to fuel temperature since heat can be directly deposited into the coolant by nuclear radiation.

Transfer function *C*, which is the other part of the transfer function of coolant temperature to the power, has been calculated as Equation (4.26). It is plotted as Figure 5.7. Again, using the insert line and data cursor functions in MATLAB for

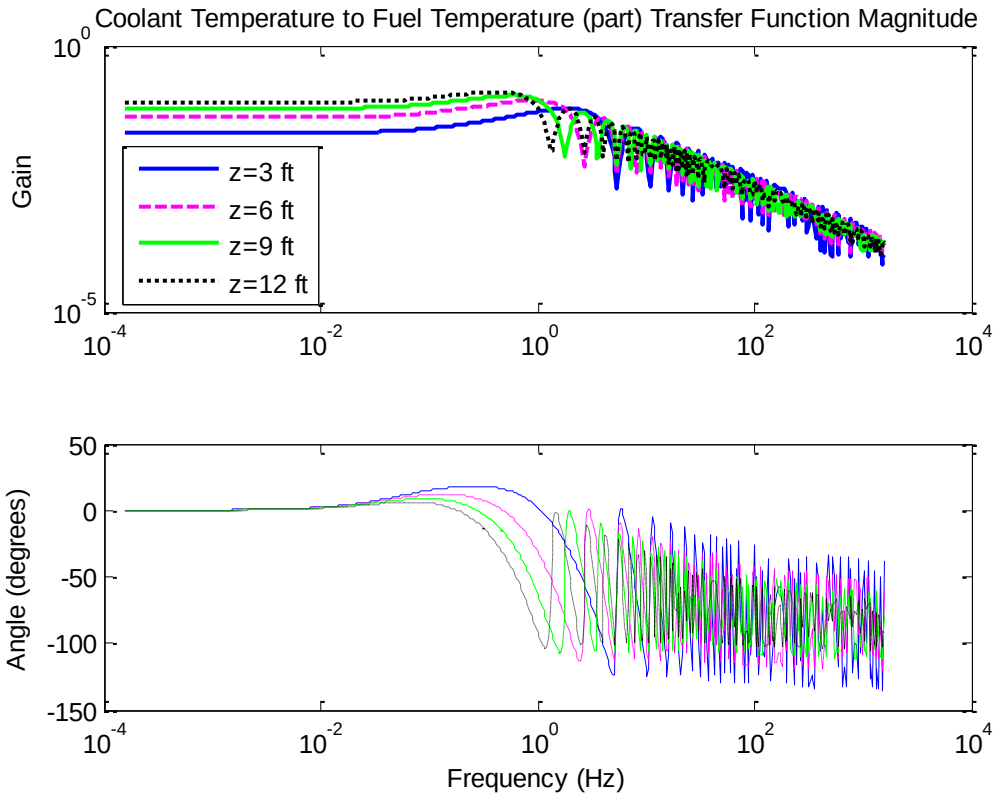

Fig. 5.6 Part of coolant temperature to fuel temperature transfer function.

the curve when z = 12 ft, like in Chapter III, it shows that the curve hits a pole at 0.207 Hz and turns to decay one decade per decade. Checking with Table 3.1, we find out that it is caused by the coolant residence time in the core (τ_R), which means if the change in power is at a low frequency, the change in coolant temperature can follow up with the change in power. However, if the frequency of change in power is increased to faster than the coolant residence time in the core, then the coolant would not be able to react with the power change because it is changing too fast.

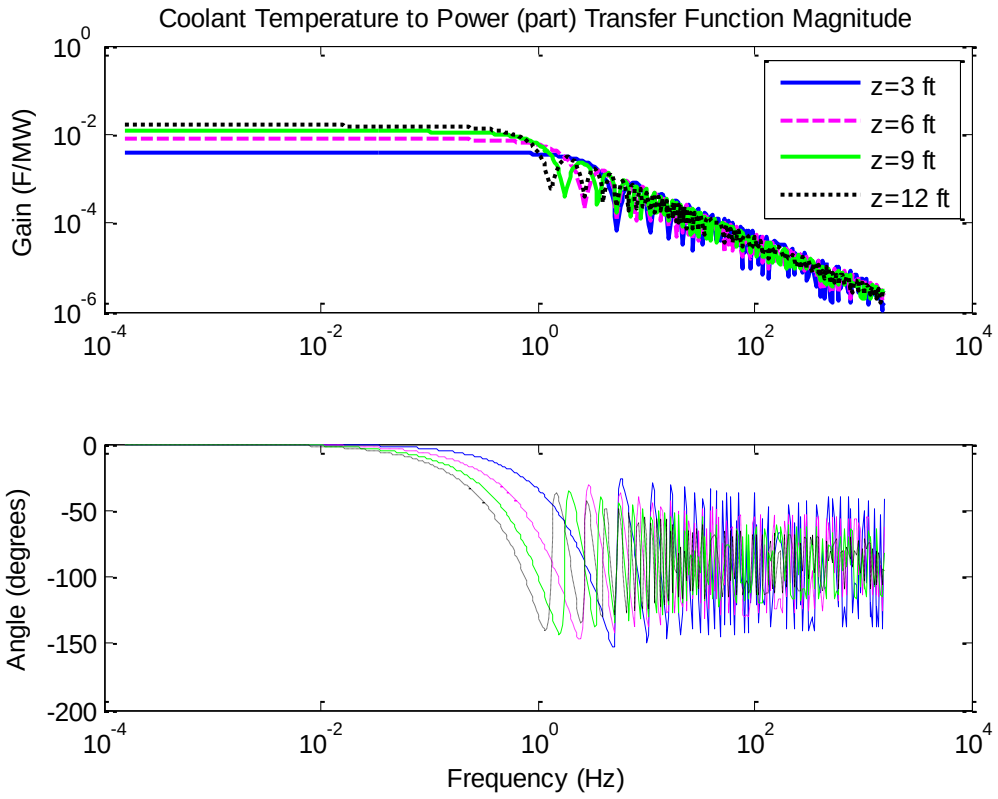

Fig. 5.7 Part of the coolant temperature to power transfer function.

From Equation (4.25), transfer function *D* in Figure 5.1, which is the coolant temperature at height z to the coolant inlet temperature $\frac{\Theta(z,s)}{\Theta_0(s)}$ can be determined, shown as Figure 5.8. As a comparison, the plot for the multi-lump model has been shown again as Figure 5.9 and Figure 5.8 has been changed to a semi-log scale for the gain and a linear scale for the angle, shown as Figure 5.10. They all show that the gains at the low frequency are close to one and they have a break frequency at 0.2056 Hz which is caused by the coolant residence time τ_R according to Table 3.1. Compare Figure 5.9 and 5.10 and find that the curves in

the distributed parameter model do not decay as fast or in the same manner as those of the multi-lump model. This is because the distributed parameter model provides an exact inclusion of the pure time delay of the coolant flow. Another reason is that the transfer function *D* has no feedback mechanism included but the multi-lump model does, as presented in Chapter III. Therefore, with the distributed parameter model, we are able to isolate on this *D* transfer function and research its effect by itself.

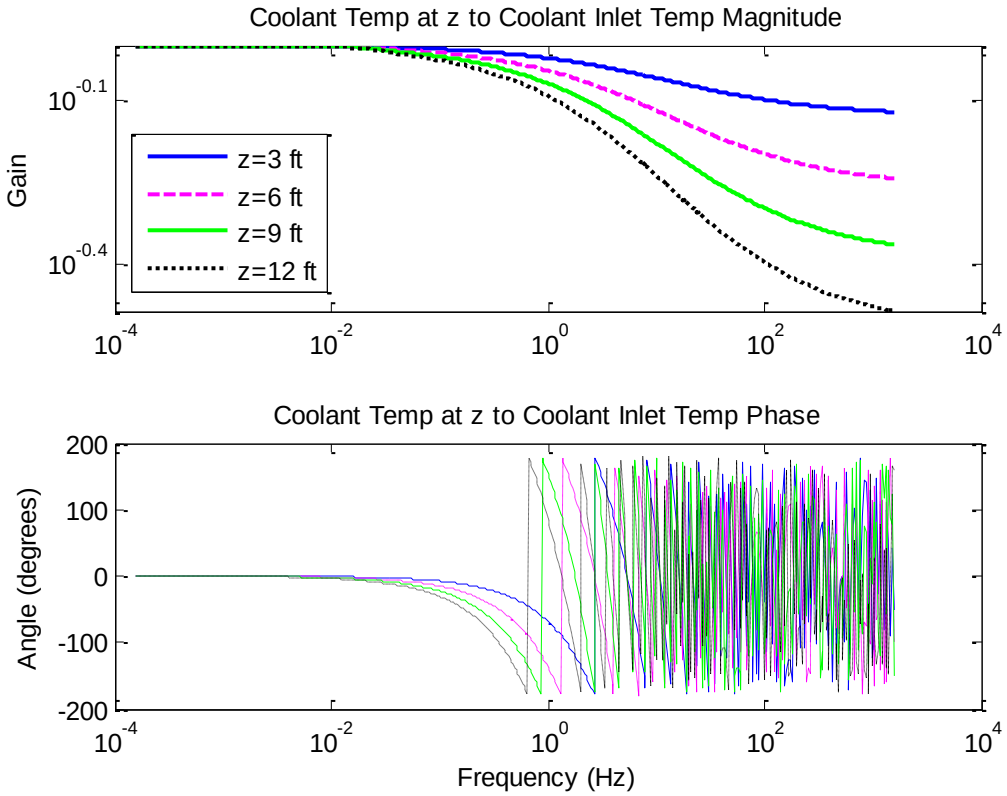

Fig. 5.8 Coolant temperature at height *z* to coolant inlet temperature - distributed-parameter log-log scale.

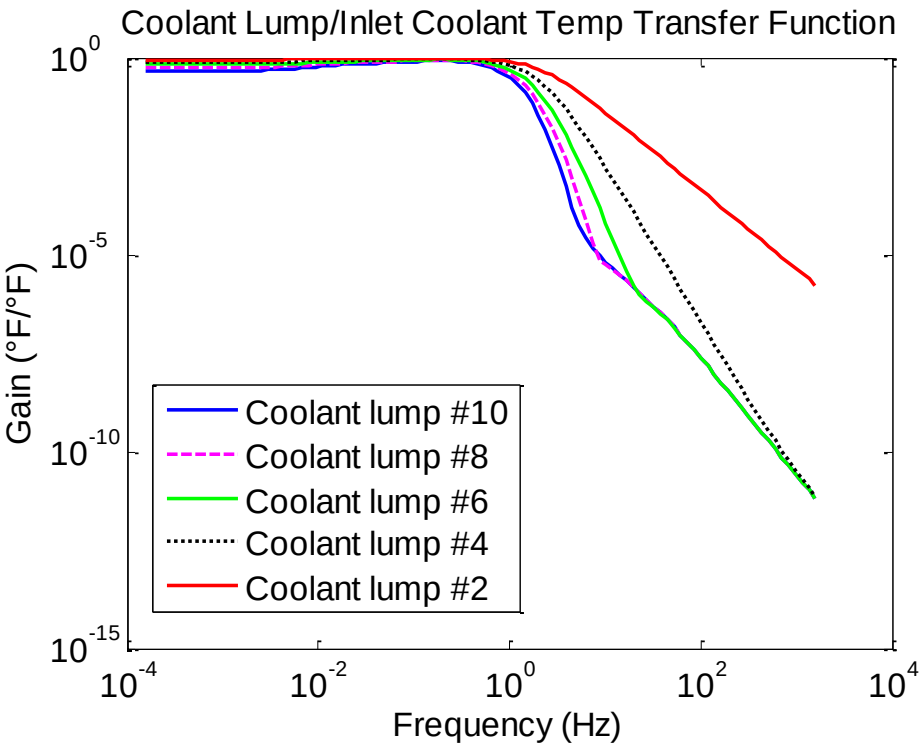

Fig. 5.9 Coolant lump temperature to coolant inlet temperature – multi node.

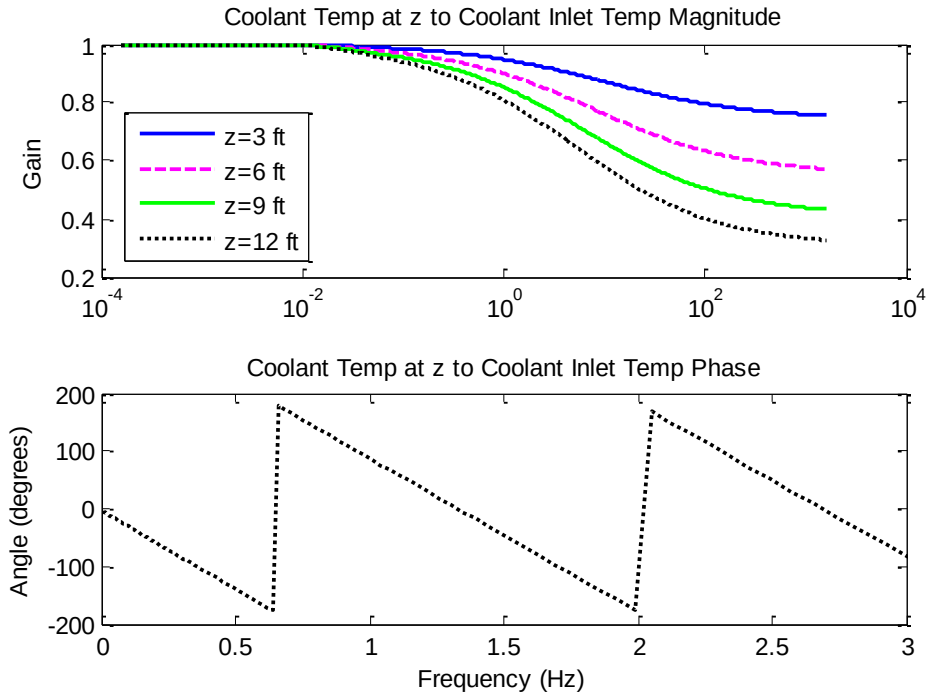

Fig. 5.10 Coolant temperature at height *z* to coolant inlet temperature - distributed-parameter compare.

Pure Time Delay

Figure 5.11 shows the pure time delay of $\tau_R = 0.76219$ second. The pure time delay is defined as: [18]

$$y_2(t) = y_1(t-\tau) \tag{5.11}$$

where y_i is the measurement at position *i*. The Laplace transform of Equation 5.11 is:

$$Y_2(s) = Y_1(s)e^{-s\tau} \tag{5.12}$$

Therefore, the transfer function between signals 1 and 2 is:

$$H(s) = \frac{Y_2(s)}{Y_1(s)} = e^{-s\tau} \tag{5.13}$$

The magnitude of the transfer function can be calculated as:

$$\left|H(j\omega)\right|^2 = H(j\omega)H^*(j\omega) = H(j\omega)H(-j\omega) = e^{-j\omega\tau}e^{j\omega\tau} = 1 \tag{5.14}$$

Thus the magnitude of the pure time delay is not very useful since it equals 1 at all frequencies. However, the magnitude of Figure 5.11 equals to 1 as well. It proves the plot is correct.

According to the Euler's formula $e^{-j\omega\tau} = \cos(-\omega\tau) + j\sin(-\omega\tau)$, the phase angle of the pure time delay can be written as:

$$\theta = \arctan\left[\frac{\mathrm{Re}(e^{-j\omega\tau})}{\mathrm{Im}(e^{-j\omega\tau})}\right] = \arctan\left[\frac{\cos(-\omega\tau)}{\sin(-\omega\tau)}\right] = \arctan\left[\tan(-\omega\tau)\right] = -\omega\tau = -2\pi f\tau \tag{5.15}$$

Thus, the slope of the phase angle versus frequency is the time delay. From Figure 5.11, the phase angle is -540° at 1.968 Hz. Therefore, $\tau = \frac{-3\pi}{(-2\pi)\times(1.968Hz)}$ $= 0.76220\,\mathrm{sec}$, which matches with the coolant residence time τ_R of the model

perfectly. Compare the phase angle plot of Figure 5.10 when z = 12 ft to the phase angle plot of Figure 5.11 and find out that the slopes of the two curves are same. This means that τ_R value from the model simulation matches with the theoretical calculation value.

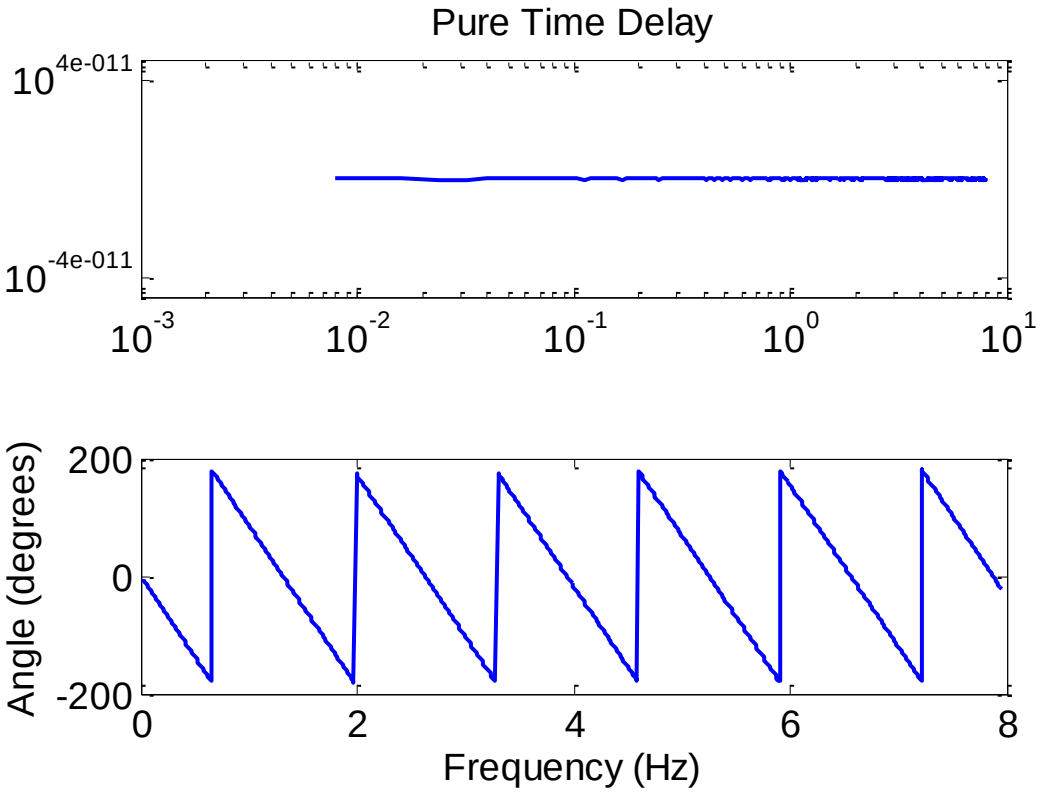

Fig. 5.11 Pure time delay of $\tau_R = 0.76219$ sec.

Combined Transfer Functions

Now, since all the individual transfer functions in Figure 5.1 have been calculated and plotted, combined transfer functions can be derived and plotted with these known equations.

From Equation (5.8), the overall transfer function of power to reactivity $\frac{\delta P}{\delta \rho_{ext}}$ can be plotted using MATLAB, shown as Figure 5.12. Figure 5.13 is the plot of the same transfer function using the multi-lump model. Compare these two figures with the plot of the zero power transfer function of Figure 5.2; they clearly show that with all the feedback mechanisms, the gain at the low frequency has been brought back to a reasonable value compared to the very large value in the zero-power transfer function. The poles and zero are still the same. The gain of Figure 5.12 at the low frequency is 31660 for z = 12 and it is 40190 for Figure 5.13. They both have a gain value of about 52250 at the plateau region and then they both hit a break frequency at 31.98 Hz, which is as same as the zero power transfer function. Then, they both decay one decade per decade. Notice that there is an obvious difference between the gains at the low frequency. This is because the multi-lump model is based on the average method. Hence, the change in power is the change in average power instead of the power at the core outlet. Therefore, it should be compared with the gain when z = 6, which is approximately at the middle of the core. Using the data cursor function in MATLAB, we find out that the gain at low frequency for z = 6 is 39650, which is close to the value of the multi-lump model.

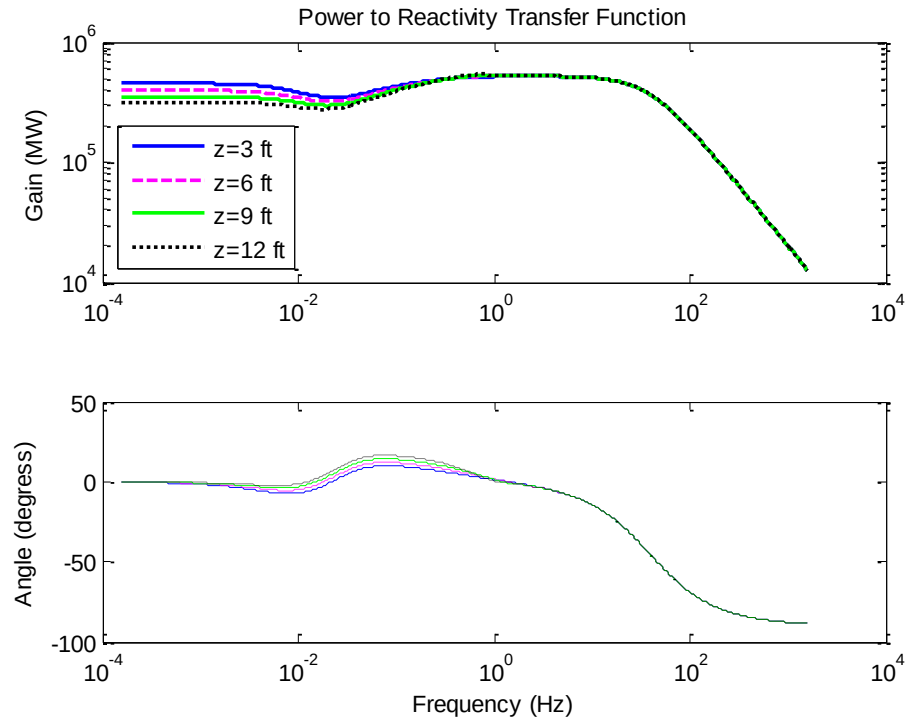

Fig. 5.12 Overall power to reactivity transfer function - distributed-parameter.

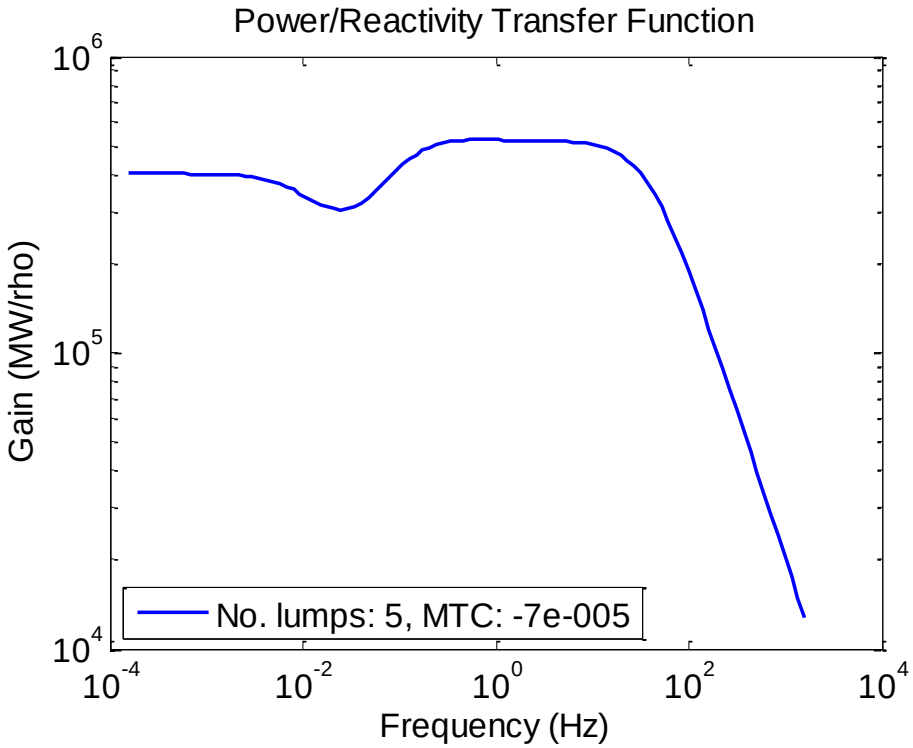

Fig. 5.13 Overall power to reactivity transfer function - multi node.

Similarly, the transfer function between power and coolant inlet temperature can be plotted according to Equation (5.9), shown as Figure 5.14; and Figure 5.15 is the plot of multi-lump model for comparison. Again, the curve when z = 6 ft is chosen to make the comparison for the same reason as Figure 5.12. The gains at the low frequency are 27.75 and 32.88, respectively. They both have a break frequency of 37.63 Hz, which again, is caused by the zero power transfer function.

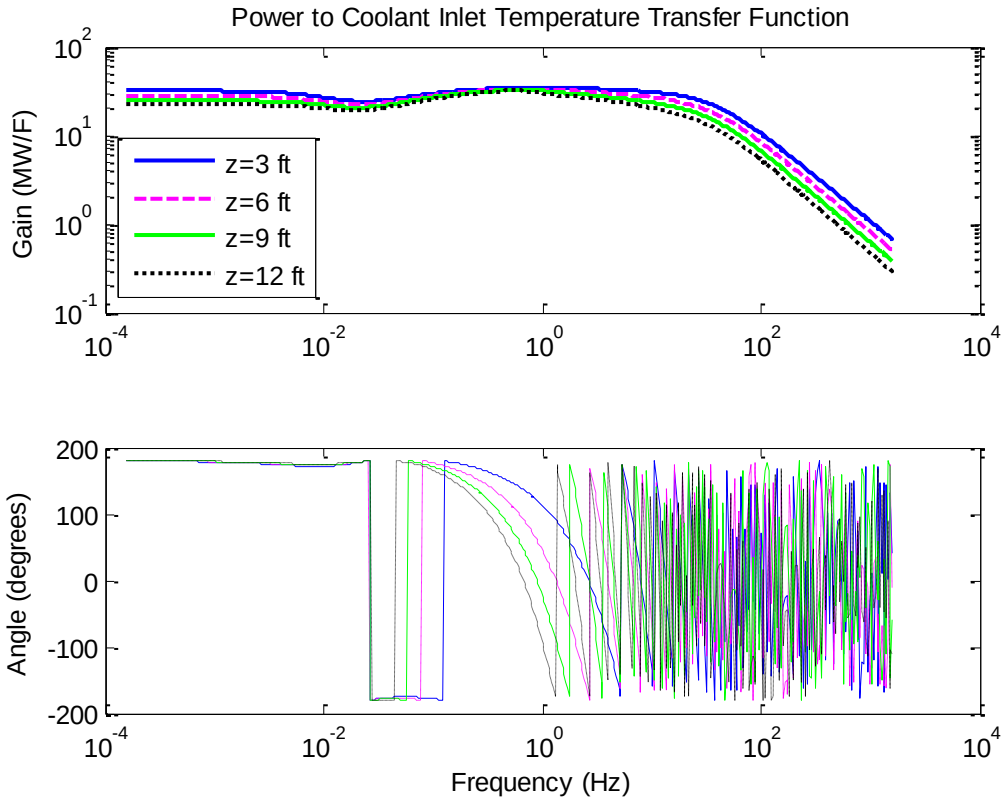

Fig. 5.14 Power to coolant inlet temperature transfer function - distributed-parameter.

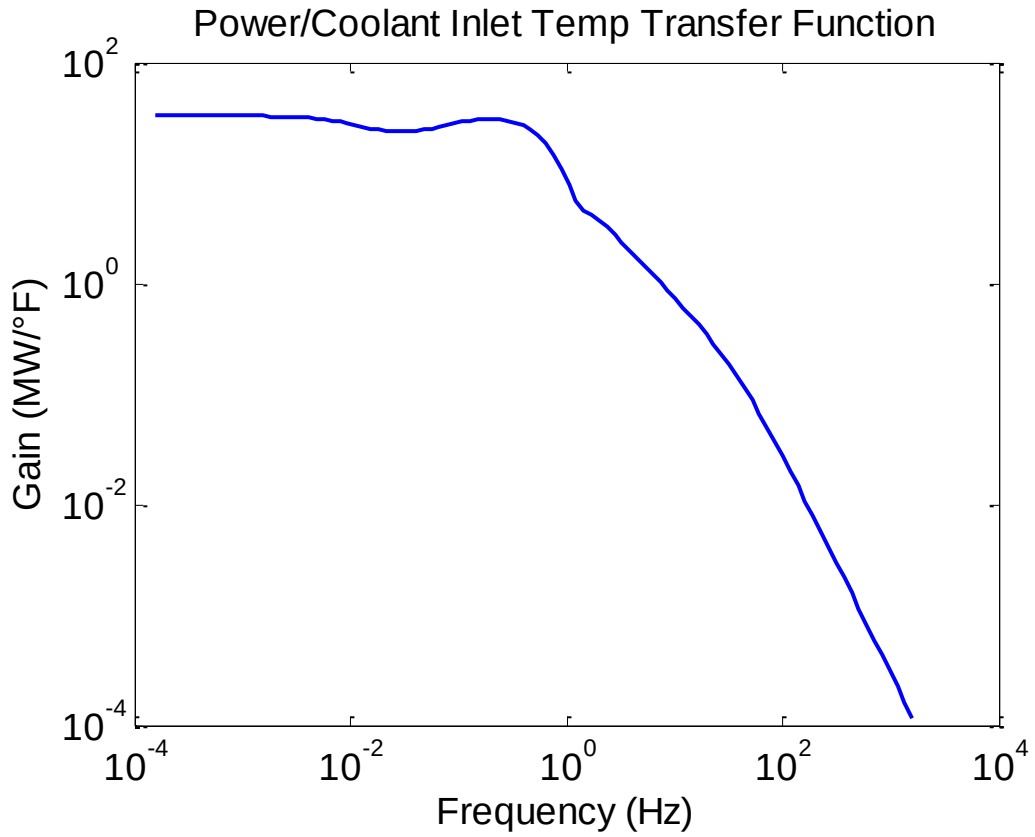

Fig. 5.15 Power to coolant inlet temperature transfer function - multi node.

The transfer function of the coolant temperature to power can be determined as well. It is the transfer function *d* in Figure 5.1. When change in reactivity is the driving source, $d = b + c + f = AB + C + 0$. Thus, it can be plotted as Figure 5.16. Figure 5.17 is the plot of the multi-lump model as a comparison. Figure 5.16 shows that the closer to the exit, the higher the coolant temperature is and the gain at the low frequency for the coolant exit is 0.01561 while it is 0.01634 in Figure 5.17, which is close. They both have a turning point at around 0.0223 Hz, which corresponds to the coolant heat transfer time constant. There is also a slight difference between two graphs. Again, as presented for Figure 5.8, it is because in

the distributed parameter model, this graph shows the transfer function that the coolant loop has been isolated from the whole system, which means it is only the *AB+C* in Figure 5.1, without all the feedback effects. However, in the multi node model, the coolant loop has not been isolated that the interaction between the coolant and fuel and the feedback changed the character of the graph. At first this may appear to be a disadvantage of the distributed parameter model, when, in fact, it is an advantage for research since individual components and physical mechanisms can be studied with the distributed parameter system while the matrix formulation of the multi-lump model makes this difficult and may cause the inaccuracy.

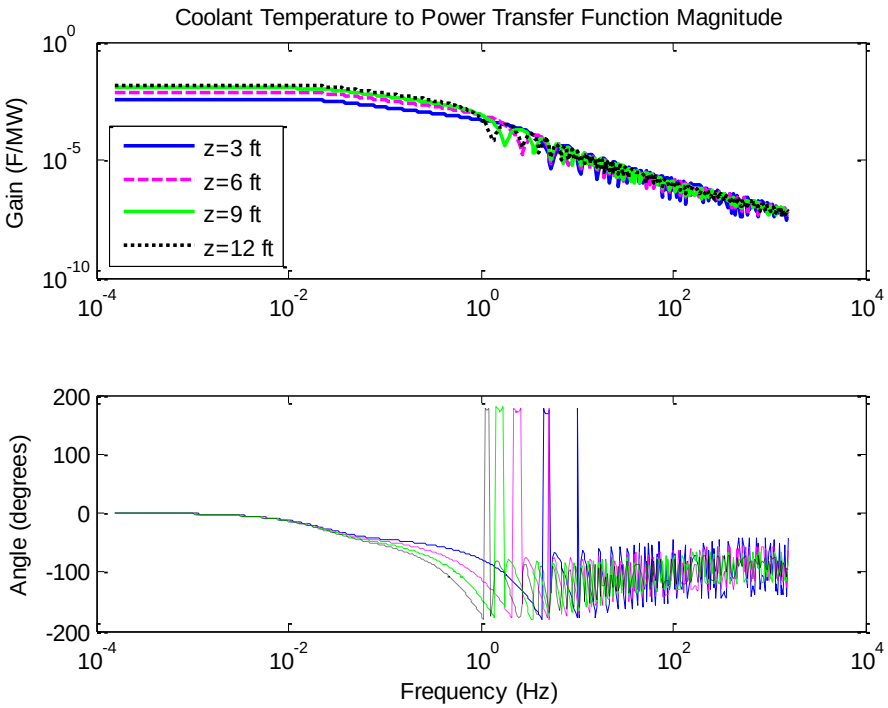

Fig. 5.16 Coolant temperature at height *z* to power transfer function - distributed-parameter.

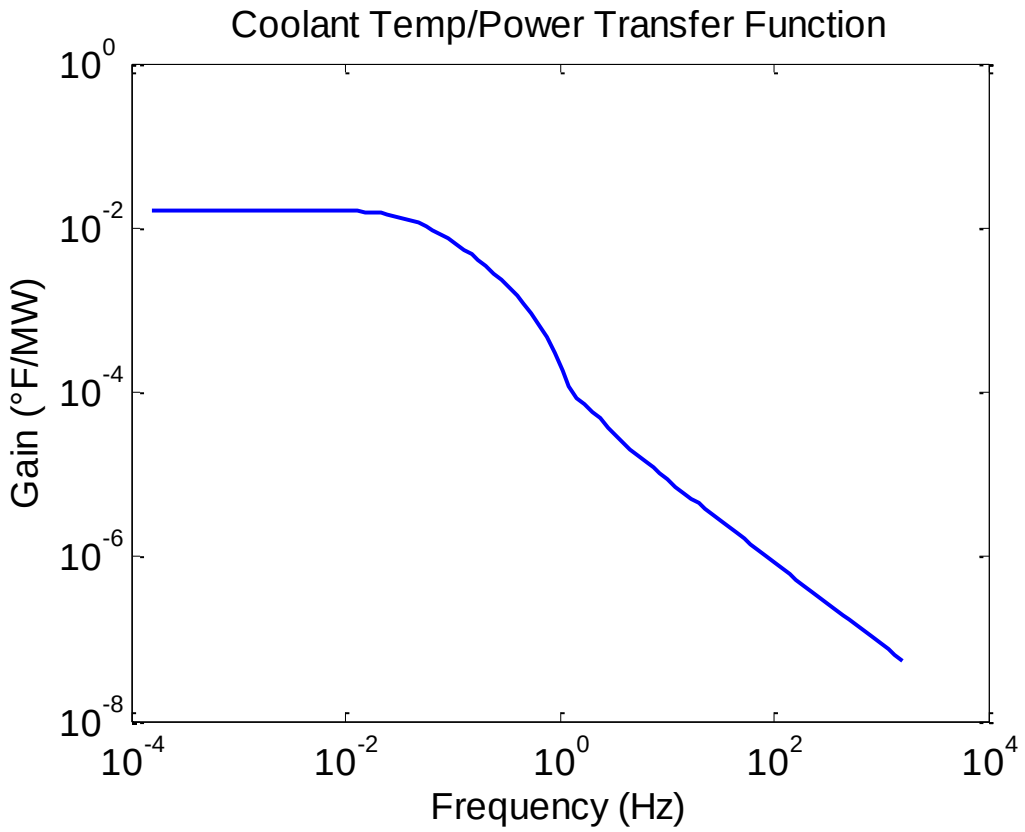

Fig. 5.17 Coolant exit temperature to power transfer function - multi node.

Then, the transfer function of coolant temperature to fuel temperature can be derived with the transfer function above.

$$\frac{\delta\Theta}{\delta T_F} = \frac{\delta\Theta}{\delta P} \times \frac{\delta P}{\delta T_F} = \frac{AB + C}{A} \tag{5.16}$$

Thus, according to Equation (5.11), the transfer function of coolant temperature to fuel temperature is plotted, shown as Figure 5.18. Again, the plot of the multi-lump model is used for comparison as Figure 5.19. The gain of Figure 5.18 is 0.0870 when $z = 12$ while it is 0.1003 for Figure 5.19 at the low frequency, which is similar. The shapes of two figures match well since they both have a gain about 0.1 at low frequency; then they hit a turning point at around

1.232 Hz. After that, the gain of Figure 5.19 drops to 0.015 after the break frequency, while the average gain value of Figure 5.18 at high frequency is also around 0.015.

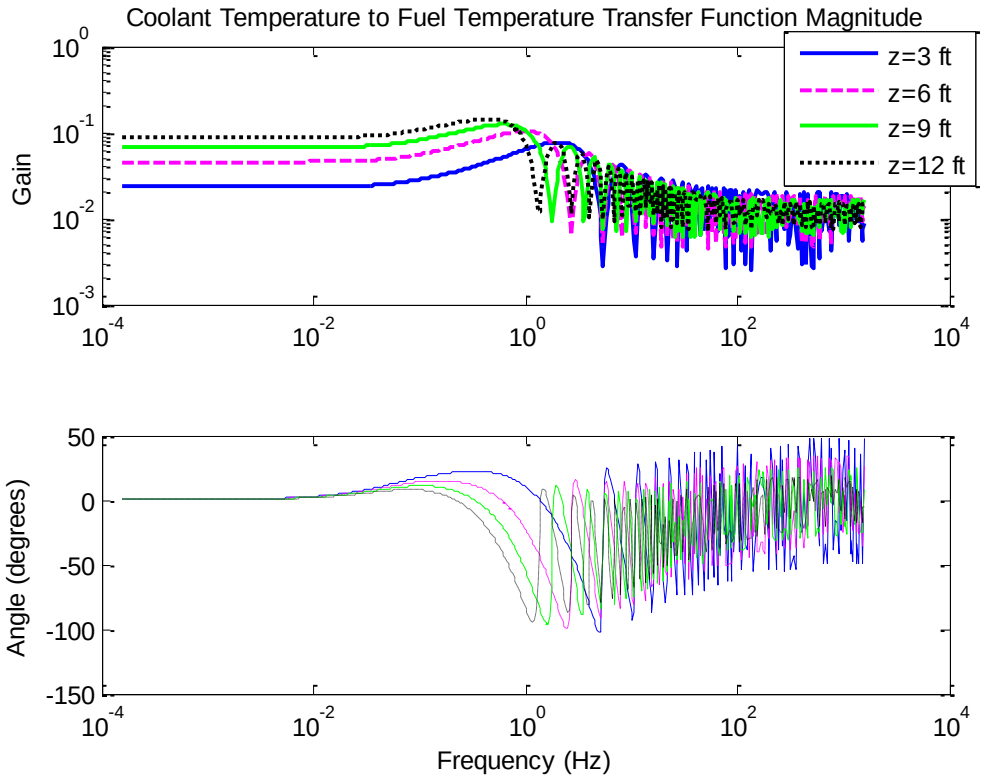

Fig. 5.18 Coolant temperature to fuel temperature transfer function - distributed-parameter.

The transfer function between fuel temperature and reactivity when change in reactivity is the driving source can be derived from Figure 5.1:

$$\frac{\delta T_F}{\delta \rho_{ext}} = \frac{a}{x-e} = \frac{xG_0A}{x-\left[\alpha_F xG_0A+\alpha_M xG_0(AB+C)+\alpha_M D\delta\theta_0\right]} \tag{5.17}$$

Since the change in reactivity is the driving source, $\delta\theta_0 = 0$. Thus,

$$\frac{\delta T_F}{\delta \rho_{ext}} = \frac{G_0A}{1-\left[\alpha_F G_0A+\alpha_M G_0(AB+C)\right]} \tag{5.18}$$

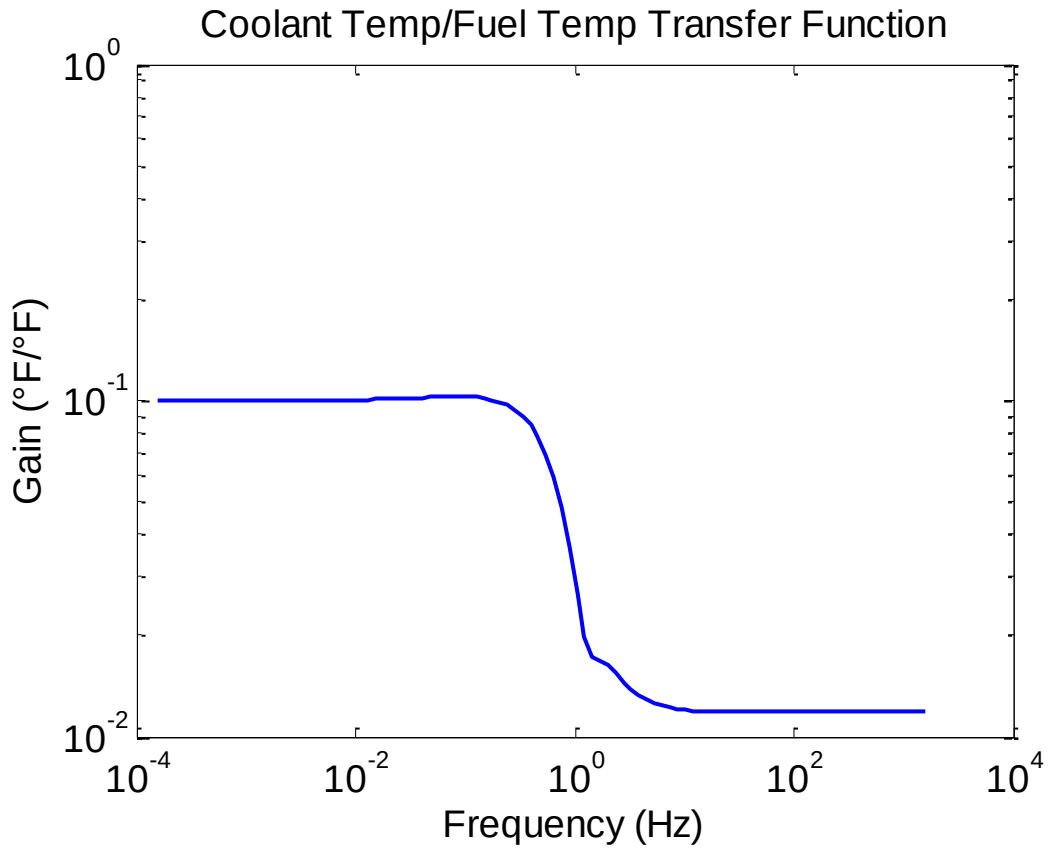

Fig. 5.19 Coolant exit temperature to fuel temperature at the upmost lump transfer function - multi node.

Figures 5.20 and 5.21 show the transfer function of fuel temperature to reactivity using distributed model and multi-lump model, respectively. These two figures match well. The gain at the low frequency is 5542 for Fig 5.20 when z = 12 and 6583 for Figure 5.21. Again, the difference at the gain is caused by the feedback mechanisms. In the distributed parameter model, the fuel and moderator temperature reactivity feedback are based on temperatures for the specific height under study. However, in the multi-lump model, all the feedback mechanisms through the core are incorporated. Both curves hit the first pole at 0.551 Hz, which corresponds to the fuel heat transfer time constant introduced in Table 3.1.

Then, they both have a break frequency at 37.64 Hz which is caused by the zero power transfer function G_0. After that, it decays from one decade per decade to two decades per decade.

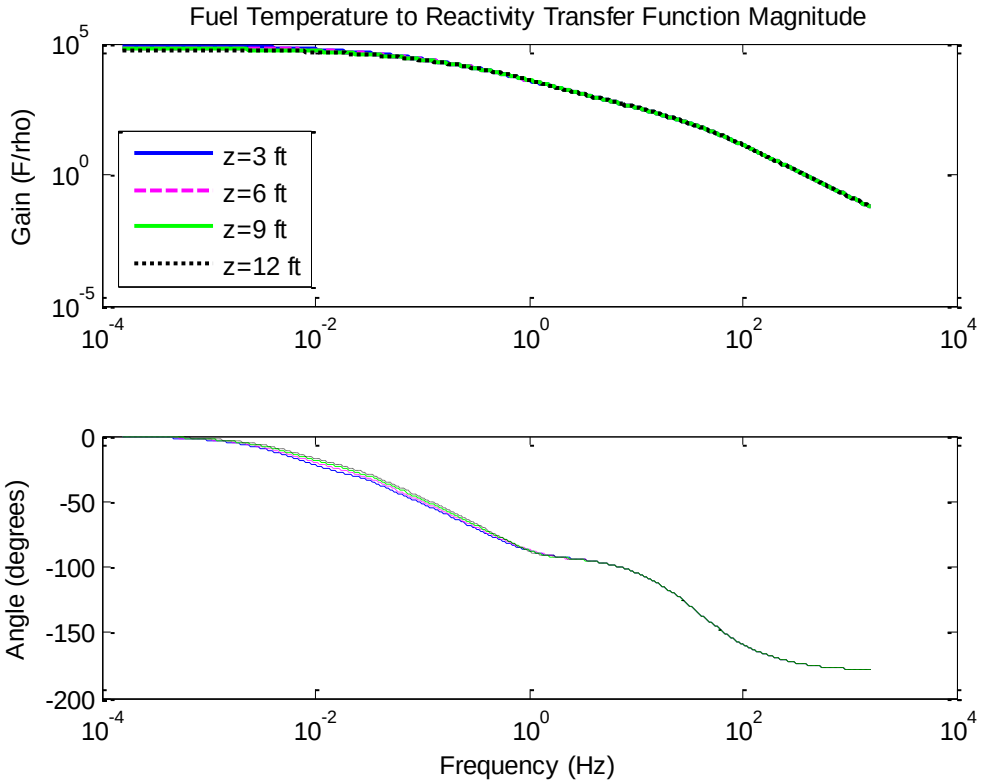

Fig. 5.20 Fuel temperature to reactivity transfer function - distributed-parameter.

Similarly, the transfer function between coolant temperature and reactivity when change in reactivity is the driving source can be derived from Figure 5.1 as well:

$$\frac{\delta\Theta}{\delta\rho_{ext}} = \frac{d}{x-e} = \frac{xG_0(AB+C)+D\delta\theta_0}{x-\left[\alpha_F xG_0A+\alpha_M xG_0(AB+C)+\alpha_M D\delta\theta_0\right]} \tag{5.19}$$

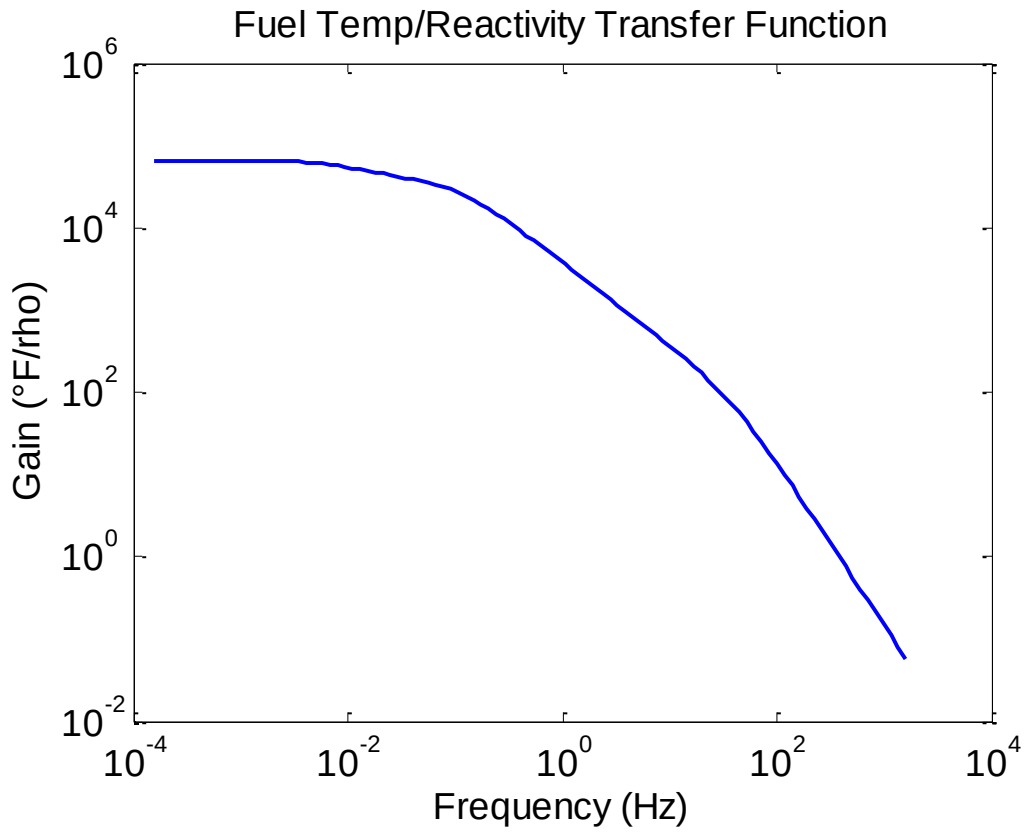

Fig. 5.21 Fuel temperature at the upmost lump to reactivity transfer function - multi node.

Still, the change in reactivity is the driving source, $\delta\theta_0 = 0$. Hence,

$$\frac{\delta\Theta}{\delta\rho_{ext}} = \frac{G_0(AB+C)}{1-\left[\alpha_F G_0 A + \alpha_M G_0(AB+C)\right]} \tag{5.20}$$

Plot Equation (5.20) using MATLAB and get the transfer function between coolant temperature and reactivity shown as Figure 5.22. Similarly, the plot of the multi-lump model is compared as Figure 5.23. The gain at the low frequency is 4943 for core exit in Figure 5.22 and 6606 in Figure 5.23. Similar to Figures 5.20 and 5.21, in this case, the difference at the gain is caused by the isolation of the feedback mechanisms. In the distributed parameter model, only the fuel and

moderator temperature reactivity feedback at the certain height is counted while in the multi-lump model, the feedback mechanisms are based on average lump temperatures through the core are included.

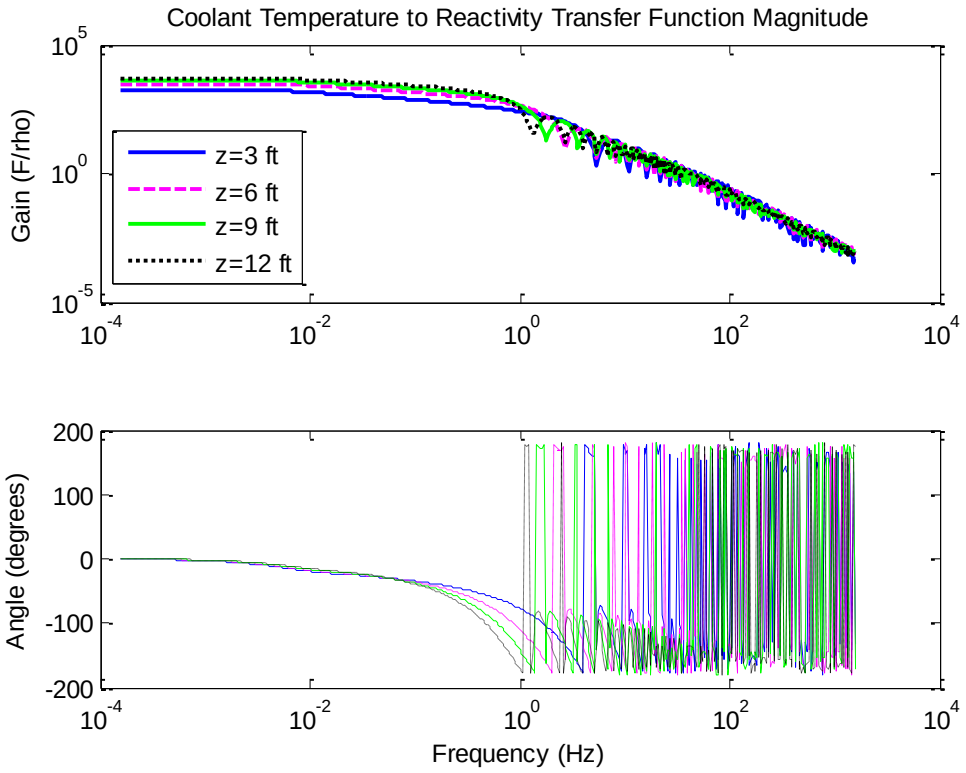

Fig. 5.22 Coolant temperature to reactivity transfer function - distributed-parameter.

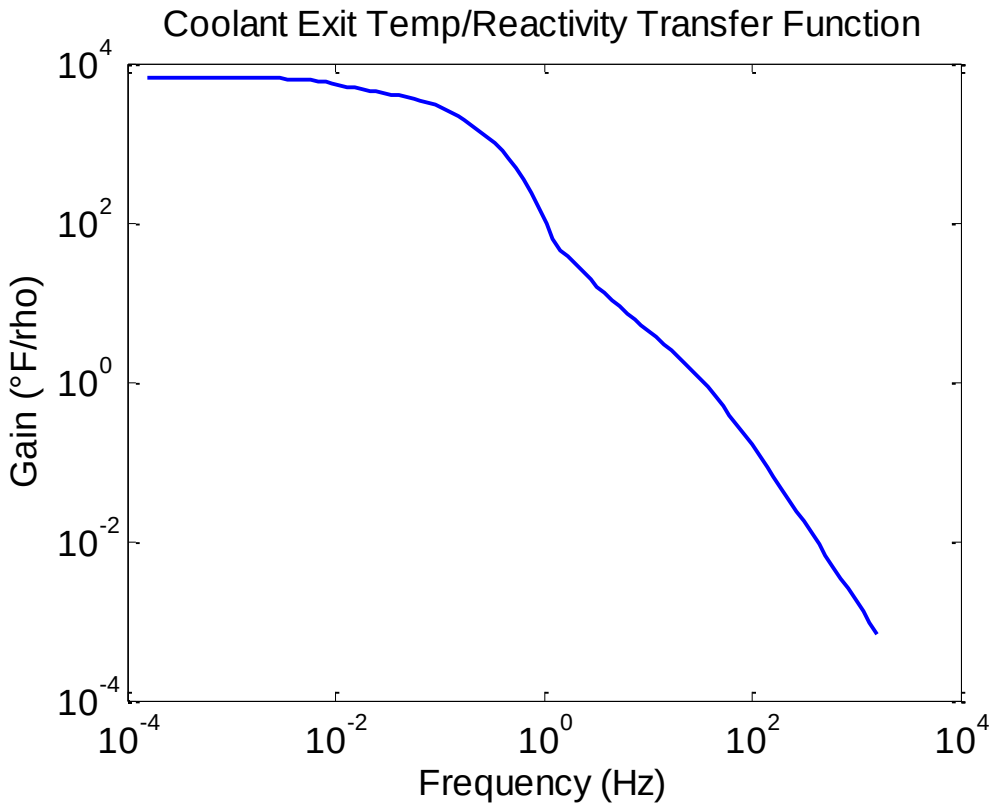

Fig. 5.23 Coolant exit temperature to reactivity transfer function - multi node.

CHAPTER VI

CONCLUSIONS AND RECOMMENDATIONS

This research concerns reactor core models built using data from the Palo Verde Nuclear Generating Station. A multi-lump model is presented using Mann's approach employing ordinary differential equations (ODEs) and a distributed parameter model is built based on partial differential equations (PDEs). Currently, commercial power plants are not inclined to accept experiments or test equipment attached to their reactor for safety reasons, except those needed for required operations. Therefore, both models are simulated and analyzed in the frequency domain with MATLAB.

From the comparisons between the multi-lump parameter model and the distributed parameter model in Chapter V, the advantages of the distributed model can be observed. Based on the methods by which the two models are established, the distributed parameter model is built upon PDEs and it has the ability to offer the transfer function at any location throughout the reactor core. However, the multi-lump parameter model is based on an average model. Hence, it can only obtain the value at a certain region (lump) instead of any specific location. Even though increasing the number of lumps can increase the model resolution, it will not change the fact that it is still based on an average method. Also, if the number of lumps is increased into a very large number, it will lead to a huge matrix, which may take a lot more (computer) time to solve while using the distributed

parameter model is much faster and easier to implement.

Another feature of the distributed parameter model is that it isolates the feedback mechanisms for the location where the research is interested. That is, only the feedbacks existing at the certain location are counted into the transfer function. In the multi-lump model, because of the matrix method it is built upon, it is inconvenient to isolate the feedbacks at the certain point and to do so will take a lot of work. Therefore, the transfer functions derived from the multi-lump model contain the feedbacks not only at a certain lump, but also the feedbacks from all over the reactor core. The advantage of this feature for the distributed parameter model is that in the research of the characteristics of a reactor core, if the feedback can be isolated for the certain point, individual components and physical mechanisms can be studied. Researchers will be able to determine what is happening at that point and what caused the effects. The drawback of this feature is that in a real reactor core, the response at a location is caused not only by the feedback mechanisms at that position but also the feedbacks happening all over the core. However, in this thesis, an assumption is made that the heat generation is uniform throughout the reactor core. Therefore, the effect of this drawback for this model is small in this case, as temperatures are relatively consistent across the core.

Even so, it is very desirable that in the future, more work could be done with

the distributed parameter model so that it is able to accurately include the feedback mechanisms when non-uniform heat generation exists. Also, from the plots of the distributed parameter model in Chapter V, it can be seen that some of the graphs have an oscillatory behavior in the transfer function at the high frequency. Analytical work has been done here to ascertain what caused this oscillatory behavior and the result shows that it is most probably caused by the exponential portion (Equation 4.25) in the transfer functions of the distributed parameter model. Therefore, it is recommended that further work be performed to fully explore this phenomenon. As mentioned at the beginning of this chapter, this distributed parameter model is analyzed based upon the simulation using a computer tool (MATLAB). Since commercial power plants do not encourage experiments or test equipment attached to their reactor because of the safety consideration, it would be very helpful if future work could take existing experimental results found in the literature (e.g., from H. B. Robinson Nuclear Plant [19]) and use their data in this model and compare the results. This could promote further improvements to the model such that in the future, it could be applied to a real nuclear reactor core to examine and analyze it, and eventually be used routinely in nuclear power plants. As a case in point, this modeling effort could be applied to diagnostic and monitoring methods, such as noise analysis, for instance, to determine the moderator temperature coefficient in nuclear reactors.

REFERENCES

[1] N. Venkatesh, Validation of Noise Analysis Techniques for Evaluationg the Moderator Temperature Coefficient in Pressurized Water Reactors, Arizona State University, 1993, pp. 19-20.

[2] "1.3 Comparison Tables," in *Palo Verde Nuclear Generating Station Final Safety Analysis Report*, 1981, pp. 1-16.

[3] S. Glasstone and A. Sesonske, "Prompt-Neutron Lifetime," in *Nuclear Reactor Engineering*, 3rd ed., Van Nostrand Reinhold Company, 1981, p. 232.

[4] J. R. Larmarsh and A. J. Baratta, "Prompt Neutron Lifetime," in *Introduction to Nuclear Engineeing*, 3rd ed., Prentice Hall, 2001, pp. 330-332.

[5] J. R. Larmarsh and A. J. Baratta, "Delayed Neutron Fractions," in *Introduction to Nuclear Engineeing*, 3rd ed., Prentice Hall, 2001, p. 343.

[6] J. K. Shultis and R. E. Faw, "The Decay Constant," in *Fundamentals of Nuclear Science and Engineering*, 2nd ed., CRC Press, 2008, pp. 103-104.

[7] J. R. Larmarsh and A. J. Baratta, "Reactor with Delayed Neutrons," in *Introduction to Nuclear Engineeing*, 3rd ed., Prentice Hall, 2001, pp. 336-337.

[8] J. Lewins, "Reactivity Units," in *Nuclear Reactor Kinetics and Control*, 1st ed., Pergamon Press, 1978, pp. 58-59.

[9] C. D. G. King, "Reactor Transient Behavior," in *Nuclear Power Systems*, The Macmillan Company, 1964, pp. 101-111.

[10] J. J. Duderstadt and L. J. Hamilton, "The Point Reactor Kinetics Model," in *Nuaclear Reactor Analysis*, John Wiley & Sons, Inc., 1976, pp. 235-241.

[11] T. W. Kerlin, "Dynamic Analysis and Control of Pressurized Water Reactors," *Control and Dynamic Systems*, vol. 14, pp. 103-212, 1978.

[12] J. J. Duderstadt and L. J. Hamilton, "Inherent Reactivity Effects," in *Nuaclear Reactor Analysis*, John Wiley & Sons, Inc., 1976, pp. 556-563.

[13] J. R. Larmarsh and A. J. Baratta, "Nuclear Doppler Effect," in *Introduction to Nuclear Engineeing*, 3rd ed., Prentice Hall, 2001, pp. 267-370.

[14] T. W. Kerlin, "Dynamic Anlaysis and Control of Pressurized Water Reactors," *Control and Dynamic Systems*, vol. 14, pp. 103-212, 1978.

[15] K. E. Holbert, "Mann's Model," in *Dynamics7 - Power Plant Modeling*, Arizona State University, 2010, pp. 11-13.

[16] K. E. Holbert, "Multi-Lump Reactor Core with Mann's Model," in *Dynamics7 - Power Plant Modeling*, 2010, pp. 13-14.

[17] K. E. Holbert, "Distributed Systems," in *Dynamics8 - Advanced Topics*, 2012, pp. 10-14.

[18] K. E. Holbert, "Linear Systems," in *Noise Analysis Tutorial*, 2010, p. 14.

[19] T. W. Kerlin, E. M. Katz, J. G. Thakkar and J. E. Strange, "Theoretical and Experimental Dynamic Analysis of the H. B. Robinson Nuclear Plant," *Nuclear Technology*, vol. 30, pp. 299-316, 1976.

APPENDIX A

PARAMETERS FOR PALO VERDE NUCLEAR GENERATING STATION

Table A

Parameters for Palo Verde nuclear generating station [1] [2]

Variable	Description	Value
h	Fuel to coolant heat transfer coefficient	6300 Btu/(hr·ft^2·°F)
p	Pitch	0.605 in.
d	Fuel rod diameter	0.382 in.
ρ_c	Coolant density	43.387 lb/ft^3
c_{pc}	Coolant specific heat	1.4159 Btu/(lb·°F)
V_c	Coolant volume in core	715.741 ft^3
k	Fuel thermal conductivity	2.17253 Btu/(hr·ft^2·°F)
m_F	Fuel mass	257100 lbm
c_{pF}	Fuel specific heat	0.07878 Btu/(lb·°F)
u	Coolant velocity in core	16.4 ft/sec
λ	Decay constant	0.1 /sec
β	Delayed neutron fraction	0.0073
Λ	Generation time	0.00003 sec
P_0	Initial or maximum power	3800 MW
α_M	Moderator temperature coefficient	-0.00007 /°F
α_F	Fuel temperature coefficient	-0.0000118 /°F
f	Fraction of heat generated in fuel	97.5%

TABLE A cont.

τ_F	Fuel heat transfer time constant	3.265 sec
τ_C	Coolant heat transfer time constant	7.087 sec
τ_R	Coolant residence time in the core (τ_R)	0.7622 sec
$(mc_p)_F$	Fuel heat capacity	20250 Btu/°F
$(mc_p)_c$	Coolant heat capacity	43963.69 Btu/°F